

The ANTARES collaboration

A. Albert^{1,2}, S. Alves³, M. André⁴, M. Anghinolfi⁵, M. Ardid⁷, S. Ardid⁷, J.-J. Aubert⁸, J. Aublin⁹, B. Baret⁹, S. Basa¹⁰, B. Belhorma¹¹, M. Bendahman^{9,12}, V. Bertin⁸, S. Biagi¹³, M. Bissinger⁶, J. Boumaaza¹², M. Bouta¹⁴, M.C. Bouwhuis¹⁵, H. Brânzaş¹⁶, R. Bruijn^{15,17}, J. Brunner⁸, J. Busto⁸, B. Caiiffi⁵, D. Calvo³, A. Capone^{18,19}, L. Caramete¹⁶, J. Carr⁸, V. Carretero³, S. Celli^{18,19}, M. Chabab²⁰, T.N. Chau⁹, R. Cherkaoui El Moursli¹², T. Chiarusi²¹, M. Circella²², A. Coleiro⁹, R. Coniglione¹³, P. Coyle⁸, A. Creusot⁹, A.F. Díaz²³, C. Distefano¹³, I. Di Palma^{18,19}, A. Domi^{15,17}, C. Donzaud^{9,24}, D. Dornic⁸, D. Drouhin^{1,2}, T. Eberl⁶, T. van Eeden¹⁵, D. van Eijk¹⁵, N. El Khayati¹², A. Enzenhöfer⁸, P. Fermani^{18,19}, G. Ferrara¹³, F. Filippini^{21,25}, L.A. Fusco⁸, Y. Gatelet⁹, P. Gay^{26,9}, H. Glotin²⁷, R. Gozzini³, R. Gracia Ruiz¹⁵, K. Graf⁶, C. Guidi^{5,28}, S. Hallmann⁶, H. van Haren²⁹, A.J. Heijboer¹⁵, Y. Hello³⁰, J.J. Hernández-Rey³, J. Hökl⁶, J. Hofestädt⁶, F. Huang⁸, G. Illuminati^{9,21,25}, C.W. James³¹, B. Jisse-Jung¹⁵, M. de Jong^{15,32}, P. de Jong^{15,17}, M. Kadler³³, O. Kalekin⁶, U. Katz⁶, N.R. Khan-Chowdhury³, A. Kouchner⁹, I. Kreykenbohm³⁴, V. Kulikovskiy⁵, R. Lahmann⁶, R. Le Breton⁹, S. LeStum⁸, D. Lefèvre³⁵, E. Leonora³⁶, G. Levi^{21,25}, D. Lopez-Coto³⁷, S. Loucatos^{38,9}, L. Maderer⁹, J. Manczak³, M. Marcelin¹⁰, A. Margiotta^{21,25}, A. Marinelli³⁹, J.A. Martínez-Mora⁷, B. Martino⁸, K. Melis^{15,17}, P. Migliozzi³⁹, A. Moussa¹⁴, R. Muller¹⁵, L. Nauta¹⁵, S. Navas³⁷, E. Nezri¹⁰, B. O’Fearraigh¹⁵, A. Păun¹⁶, G.E. Păvălaş¹⁶, C. Pellegrino^{21,40,41}, M. Perrin-Terrin⁸, V. Pestel¹⁵, P. Piattelli¹³, C. Pieterse³, C. Poiré⁷, V. Popa¹⁶, T. Pradier¹, N. Randazzo³⁶, D. Real³, S. Reck⁶, G. Riccobene¹³, A. Romanov^{5,28}, A. Sánchez-Losa^{3,22}, F. Salesa Greus³, D. F. E. Samtleben^{15,32}, M. Sanguineti^{5,28}, P. Sapienza¹³, J. Schnabel⁶, J. Schumann⁶, F. Schüssler³⁸, J. Seneca¹⁵, M. Spurio^{21,25}, Th. Stolarczyk³⁸, M. Taiuti^{5,28}, Y. Tayalati¹², S.J. Tingay³¹, B. Vallage^{38,9}, V. Van Elewyck^{9,42}, F. Versari^{21,25,9}, S. Viola¹³, D. Vivolo^{39,43}, J. Wilms³⁴, S. Zavatarelli⁵, A. Zegarelli^{18,19}, J.D. Zornoza³, J. Zúñiga³

¹ *Université de Strasbourg, CNRS, IPHC UMR 7178, F-67000 Strasbourg, France.*

² *Université de Haute Alsace, F-68100 Mulhouse, France.*

³ *IFIC - Instituto de Física Corpuscular (CSIC - Universitat de València) c/ Catedrático José Beltrán, 2 E-46980 Paterna, Valencia, Spain.*

⁴ *Technical University of Catalonia, Laboratory of Applied Bioacoustics, Rambla Exposició, 08800 Vilanova i la Geltrú, Barcelona, Spain.*

⁵ *INFN - Sezione di Genova, Via Dodecaneso 33, 16146 Genova, Italy.*

⁶ *Friedrich-Alexander-Universität Erlangen-Nürnberg, Erlangen Centre for Astroparticle Physics, Erwin-Rommel-Str. 1, 91058 Erlangen, Germany.*

⁷ *Institut d’Investigació per a la Gestió Integrada de les Zones Costaneres (IGIC) - Universitat Politècnica de València. C/ Paranimf 1, 46730 Gandia, Spain.*

⁸ *Aix Marseille Univ, CNRS/IN2P3, CPPM, Marseille, France.*

⁹ *Université de Paris, CNRS, Astroparticule et Cosmologie, F-75013 Paris, France.*

¹⁰ *Aix Marseille Univ, CNRS, CNES, LAM, Marseille, France.*

¹¹ *National Center for Energy Sciences and Nuclear Techniques, B.P.1382, R. P.10001 Rabat, Morocco.*

¹² *University Mohammed V in Rabat, Faculty of Sciences, 4 av. Ibn Battouta, B.P. 1014, R.P. 10000 Rabat, Morocco.*

Corresponding author:

analysis@icecube.wisc.edu

- ¹³*INFN - Laboratori Nazionali del Sud (LNS), Via S. Sofia 62, 95123 Catania, Italy.*
- ¹⁴*University Mohammed I, Laboratory of Physics of Matter and Radiations, B.P.717, Oujda 6000, Morocco.*
- ¹⁵*Nikhef, Science Park, Amsterdam, The Netherlands.*
- ¹⁶*Institute of Space Science, RO-077125 Bucharest, Măgurele, Romania.*
- ¹⁷*Universiteit van Amsterdam, Instituut voor Hoge-Energie Fysica, Science Park 105, 1098 XG Amsterdam, The Netherlands.*
- ¹⁸*INFN - Sezione di Roma, P.le Aldo Moro 2, 00185 Roma, Italy.*
- ¹⁹*Dipartimento di Fisica dell'Università La Sapienza, P.le Aldo Moro 2, 00185 Roma, Italy.*
- ²⁰*LPHEA, Faculty of Science - Semlali, Cadi Ayyad University, P.O.B. 2390, Marrakech, Morocco.*
- ²¹*INFN - Sezione di Bologna, Viale Berti-Pichat 6/2, 40127 Bologna, Italy.*
- ²²*INFN - Sezione di Bari, Via E. Orabona 4, 70126 Bari, Italy.*
- ²³*Department of Computer Architecture and Technology/CITIC, University of Granada, 18071 Granada, Spain.*
- ²⁴*Université Paris-Sud, 91405 Orsay Cedex, France.*
- ²⁵*Dipartimento di Fisica e Astronomia dell'Università, Viale Berti Pichat 6/2, 40127 Bologna, Italy.*
- ²⁶*Laboratoire de Physique Corpusculaire, Clermont Université, Université Blaise Pascal, CNRS/IN2P3, BP 10448, F-63000 Clermont-Ferrand, France.*
- ²⁷*LIS, UMR Université de Toulon, Aix Marseille Université, CNRS, 83041 Toulon, France.*
- ²⁸*Dipartimento di Fisica dell'Università, Via Dodecaneso 33, 16146 Genova, Italy.*
- ²⁹*Royal Netherlands Institute for Sea Research (NIOZ), Landsdiep 4, 1797 SZ 't Horntje (Texel), the Netherlands.*
- ³⁰*Géozur, UCA, CNRS, IRD, Observatoire de la Côte d'Azur, Sophia Antipolis, France.*
- ³¹*International Centre for Radio Astronomy Research - Curtin University, Bentley, WA 6102, Australia.*
- ³²*Huygens-Kamerlingh Onnes Laboratorium, Universiteit Leiden, The Netherlands.*
- ³³*Institut für Theoretische Physik und Astrophysik, Universität Würzburg, Emil-Fischer Str. 31, 97074 Würzburg, Germany.*
- ³⁴*Dr. Remeis-Sternwarte and ECAP, Friedrich-Alexander-Universität Erlangen-Nürnberg, Sternwartstr. 7, 96049 Bamberg, Germany.*
- ³⁵*Mediterranean Institute of Oceanography (MIO), Aix-Marseille University, 13288, Marseille, Cedex 9, France; Université du Sud Toulon-Var, CNRS-INSU/IRD UM 110, 83957, La Garde Cedex, France.*
- ³⁶*INFN - Sezione di Catania, Via S. Sofia 64, 95123 Catania, Italy.*
- ³⁷*Dpto. de Física Teórica y del Cosmos & C.A.F.P.E., University of Granada, 18071 Granada, Spain.*
- ³⁸*IRFU, CEA, Université Paris-Saclay, F-91191 Gif-sur-Yvette, France.*
- ³⁹*INFN - Sezione di Napoli, Via Cintia 80126 Napoli, Italy.*
- ⁴⁰*Museo Storico della Fisica e Centro Studi e Ricerche Enrico Fermi, Piazza del Viminale 1, 00184, Roma.*
- ⁴¹*INFN - CNAF, Viale C. Berti Pichat 6/2, 40127, Bologna.*
- ⁴²*Institut Universitaire de France, 75005 Paris, France.*
- ⁴³*Dipartimento di Fisica dell'Università Federico II di Napoli, Via Cintia 80126, Napoli, Italy.*

The IceCube Collaboration

R. Abbasi¹⁷, M. Ackermann⁶¹, J. Adams¹⁸, J. A. Aguilar¹², M. Ahlers²², M. Ahrens⁵¹, J.M. Alameddine²³, C. Alispach²⁸, A. A. Alves Jr.³¹, N. M. Amin⁴³, K. Andeen⁴¹, T. Anderson⁵⁸, G. Anton²⁶, C. Argüelles¹⁴, Y. Ashida³⁹, S. Axani¹⁵, X. Bai⁴⁷, A. Balagopal V.³⁹, A. Barbano²⁸, S. W. Barwick³⁰, B. Bastian⁶¹, V. Basu³⁹, S. Baur¹², R. Bay⁸, J. J. Beatty^{20, 21}, K.-H. Becker⁶⁰, J. Becker Tjus¹¹, C. Bellenghi²⁷, S. BenZvi⁴⁹, D. Berley¹⁹, E. Bernardini^{61, 62}, D. Z. Besson^{34, 63}, G. Binder^{8, 9}, D. Bindig⁶⁰, E. Blaufuss¹⁹, S. Blot⁶¹, M. Boddenberg¹, F. Bontempo³¹, J. Borowka¹, S. Böser⁴⁰,

O. Botner⁵⁹, J. Böttcher¹, E. Bourbeau²², F. Bradascio⁶¹, J. Braun³⁹, B. Brinson⁶, S. Bron²⁸, J. Brostean-Kaiser⁶¹, S. Browne³², A. Burgman⁵⁹, R. T. Burley², R. S. Busse⁴², M. A. Campana⁴⁶, E. G. Carnie-Bronca², C. Chen⁶, Z. Chen⁵², D. Chirkin³⁹, K. Choi⁵³, B. A. Clark²⁴, K. Clark³³, L. Classen⁴², G. H. Collin¹⁵, J. M. Conrad¹⁵, P. Coppin¹³, P. Correa¹³, D. F. Cowen^{57,58}, R. Cross⁴⁹, C. Dappen¹, P. Dave⁶, C. De Clercq¹³, J. J. DeLaunay⁵⁶, D. Delgado López¹⁴, H. Dembinski⁴³, K. Deoskar⁵¹, A. Desai³⁹, P. Desiati³⁹, K. D. de Vries¹³, G. de Wasseige³⁶, M. de With¹⁰, T. DeYoung²⁴, A. Diaz¹⁵, J. C. Díaz-Vélez³⁹, M. Dittmer⁴², H. Dujmovic³¹, M. Dunkman⁵⁸, M. A. DuVernois³⁹, E. Dvorak⁴⁷, T. Ehrhardt⁴⁰, P. Eller²⁷, H. Erpenbeck¹, J. Evans¹⁹, P. A. Evenson⁴³, K. L. Fan¹⁹, A. R. Fazely⁷, A. Fedynitch⁵⁵, N. Feigl¹⁰, S. Fiedlschuster²⁶, A. T. Fienberg⁵⁸, K. Filimonov⁸, C. Finley⁵¹, L. Fischer⁶¹, D. Fox⁵⁷, A. Franckowiak^{11,61}, E. Friedman¹⁹, A. Fritz⁴⁰, P. Fürst¹, T. K. Gaisser⁴³, J. Gallagher³⁸, E. Ganster¹, A. Garcia¹⁴, S. Garrappa⁶¹, L. Gerhardt⁹, A. Ghadimi⁵⁶, C. Glaser⁵⁹, T. Glauch²⁷, T. Glüsenkamp²⁶, J. G. Gonzalez⁴³, S. Goswami⁵⁶, D. Grant²⁴, T. Grégoire⁵⁸, S. Griswold⁴⁹, C. Günther¹, P. Gutjahr²³, C. Haack²⁷, A. Hallgren⁵⁹, R. Halliday²⁴, L. Halve¹, F. Halzen³⁹, M. Ha Minh²⁷, K. Hanson³⁹, J. Hardin³⁹, A. A. Harnisch²⁴, A. Haungs³¹, D. Hebecker¹⁰, K. Helbing⁶⁰, F. Henningsen²⁷, E. C. Hettinger²⁴, S. Hickford⁶⁰, J. Hignight²⁵, C. Hill¹⁶, G. C. Hill², K. D. Hoffman¹⁹, R. Hoffmann⁶⁰, B. Hokanson-Fasig³⁹, K. Hoshina^{39,64}, M. Huber²⁷, T. Huber³¹, K. Hultqvist⁵¹, M. Hünnefeld²³, R. Hussain³⁹, K. Hyman²³, S. In⁵³, N. Iovine¹², A. Ishihara¹⁶, M. Jansson⁵¹, G. S. Japaridze⁵, M. Jeong⁵³, M. Jin¹⁴, B. J. P. Jones⁴, D. Kang³¹, W. Kang⁵³, X. Kang⁴⁶, A. Kappes⁴², D. Kappesser⁴⁰, L. Kardum²³, T. Karg⁶¹, M. Karl²⁷, A. Karle³⁹, M. Kauer³⁹, M. Kellermann¹, J. L. Kelley³⁹, A. Kheirandish⁵⁸, K. Kin¹⁶, T. Kintscher⁶¹, J. Kiryluk⁵², S. R. Klein^{8,9}, R. Koirala⁴³, H. Kolanoski¹⁰, T. Kontrimas²⁷, L. Köpke⁴⁰, C. Kopper²⁴, S. Kopper⁵⁶, D. J. Koskinen²², P. Koundal³¹, M. Kovacevich⁴⁶, M. Kowalski^{10,61}, T. Kozynets²², E. Kun¹¹, N. Kurahashi⁴⁶, N. Lad⁶¹, C. Lagunas Gualda⁶¹, J. L. Lanfranchi⁵⁸, M. J. Larson¹⁹, F. Lauber⁶⁰, J. P. Lazar^{14,39}, J. W. Lee⁵³, K. Leonard³⁹, A. Leszczyńska³², Y. Li⁵⁸, M. Lincetto¹¹, Q. R. Liu³⁹, M. Liubarska²⁵, E. Lohfink⁴⁰, C. J. Lozano Mariscal⁴², F. Lucarelli²⁸, A. Ludwig^{24,35}, W. Luszczak³⁹, Y. Lyu^{8,9}, W. Y. Ma⁶¹, J. Madsen³⁹, K. B. M. Mahn²⁴, Y. Makino³⁹, S. Mancina³⁹, I. Martinez-Soler¹⁴, R. Maruyama⁴⁴, K. Mase¹⁶, T. McElroy²⁵, F. McNally³⁷, J. V. Mead²², K. Meagher³⁹, S. Mechbal⁶¹, A. Medina²¹, M. Meier¹⁶, S. Meighen-Berger²⁷, J. Micallef²⁴, D. Mockler¹², T. Montaruli²⁸, R. W. Moore²⁵, R. Morse³⁹, M. Moulai¹⁵, R. Naab⁶¹, R. Nagai¹⁶, U. Naumann⁶⁰, J. Necker⁶¹, L. V. Nguyễn²⁴, H. Niederhausen²⁴, M. U. Nisa²⁴, S. C. Nowicki²⁴, A. Obertacke Pollmann⁶⁰, M. Oehler³¹, B. Oeyen²⁹, A. Olivas¹⁹, E. O'Sullivan⁵⁹, H. Pandya⁴³, D. V. Pankova⁵⁸, N. Park³³, G. K. Parker⁴, E. N. Paudel⁴³, L. Paul⁴¹, C. Pérez de los Heros⁵⁹, L. Peters¹, J. Peterson³⁹, S. Philippen¹, S. Pieper⁶⁰, M. Pittermann³², A. Pizzuto³⁹, M. Plum⁴¹, Y. Popovych⁴⁰, A. Porcelli²⁹, M. Prado Rodriguez³⁹, P. B. Price⁸, B. Pries²⁴, G. T. Przybylski⁹, C. Raab¹², J. Rack-Helleis⁴⁰, A. Raissi¹⁸, M. Rameez²², K. Rawlins³, I. C. Rea²⁷, A. Rehman⁴³, P. Reichherzer¹¹, R. Reimann¹, G. Renzi¹², E. Resconi²⁷, S. Reusch⁶¹, W. Rhode²³, M. Richman⁴⁶, B. Riedel³⁹, E. J. Roberts², S. Robertson^{8,9}, G. Roellinghoff⁵³, M. Rongen⁴⁰, C. Rott^{50,53}, T. Ruhe²³, D. Ryckbosch²⁹, D. Rysewyk Cantu²⁴, I. Safa^{14,39}, J. Saffer³², S. E. Sanchez Herrera²⁴, A. Sandroock²³, M. Santander⁵⁶, S. Sarkar⁴⁵, S. Sarkar²⁵, K. Satalecka⁶¹, M. Schaufel¹, S. Schindler²⁶, T. Schmidt¹⁹, A. Schneider³⁹, J. Schneider²⁶, F. G. Schröder^{31,43}, L. Schumacher²⁷, G. Schwefer¹, S. Sclafani⁴⁶, D. Seckel⁴³, S. Seunarine⁴⁸, A. Sharma⁵⁹, S. Shefali³², M. Silva³⁹, B. Skrzypek¹⁴, B. Smithers⁴, R. Snihur³⁹, J. Soedingrekso²³, D. Soldin⁴³, C. Spannfellner²⁷, G. M. Spiczak⁴⁸, C. Spiering^{61,63}, J. Stachurska⁶¹, M. Stamatikos²¹, T. Stanev⁴³, R. Stein⁶¹, J. Stettner¹, A. Steuer⁴⁰, T. Stezelberger⁹, T. Stürwald⁶⁰, T. Stuttard²², G. W. Sullivan¹⁹, I. Taboada⁶,

S. Ter-Antonyan⁷, S. Tilav⁴³, F. Tischbein¹, K. Tollefson²⁴, C. Tönemis⁵⁴, S. Toscano¹², D. Tosi³⁹, A. Trettin⁶¹, M. Tselengidou²⁶, C. F. Tung⁶, A. Turcati²⁷, R. Turcotte³¹, C. F. Turley⁵⁸, J. P. Twagirayezu²⁴, B. Ty³⁹, M. A. Unland Elorrieta⁴², N. Valtonen-Mattila⁵⁹, J. Vandenbroucke³⁹, N. van Eijndhoven¹³, D. Vannerom¹⁵, J. van Santen⁶¹, S. Verpoest²⁹, C. Walck⁵¹, T. B. Watson⁴, C. Weaver²⁴, P. Weigel¹⁵, A. Weindl³¹, M. J. Weiss⁵⁸, J. Weldert⁴⁰, C. Wendt³⁹, J. Werthebach²³, M. Weyrauch³², N. Whitehorn^{24, 35}, C. H. Wiebusch¹, D. R. Williams⁵⁶, M. Wolf²⁷, K. Woschnagg⁸, G. Wrede²⁶, J. Wulff¹¹, X. W. Xu⁷, J. P. Yanez²⁵, S. Yoshida¹⁶, S. Yu²⁴, T. Yuan³⁹, Z. Zhang⁵², P. Zhelнин¹⁴

¹ *III. Physikalisches Institut, RWTH Aachen University, D-52056 Aachen, Germany*

² *Department of Physics, University of Adelaide, Adelaide, 5005, Australia*

³ *Dept. of Physics and Astronomy, University of Alaska Anchorage, 3211 Providence Dr., Anchorage, AK 99508, USA*

⁴ *Dept. of Physics, University of Texas at Arlington, 502 Yates St., Science Hall Rm 108, Box 19059, Arlington, TX 76019, USA*

⁵ *CTSPS, Clark-Atlanta University, Atlanta, GA 30314, USA*

⁶ *School of Physics and Center for Relativistic Astrophysics, Georgia Institute of Technology, Atlanta, GA 30332, USA*

⁷ *Dept. of Physics, Southern University, Baton Rouge, LA 70813, USA*

⁸ *Dept. of Physics, University of California, Berkeley, CA 94720, USA*

⁹ *Lawrence Berkeley National Laboratory, Berkeley, CA 94720, USA*

¹⁰ *Institut für Physik, Humboldt-Universität zu Berlin, D-12489 Berlin, Germany*

¹¹ *Fakultät für Physik & Astronomie, Ruhr-Universität Bochum, D-44780 Bochum, Germany*

¹² *Université Libre de Bruxelles, Science Faculty CP230, B-1050 Brussels, Belgium*

¹³ *Vrije Universiteit Brussel (VUB), Dienst ELEM, B-1050 Brussels, Belgium*

¹⁴ *Department of Physics and Laboratory for Particle Physics and Cosmology, Harvard University, Cambridge, MA 02138, USA*

¹⁵ *Dept. of Physics, Massachusetts Institute of Technology, Cambridge, MA 02139, USA*

¹⁶ *Dept. of Physics and Institute for Global Prominent Research, Chiba University, Chiba 263-8522, Japan*

¹⁷ *Department of Physics, Loyola University Chicago, Chicago, IL 60660, USA*

¹⁸ *Dept. of Physics and Astronomy, University of Canterbury, Private Bag 4800, Christchurch, New Zealand*

¹⁹ *Dept. of Physics, University of Maryland, College Park, MD 20742, USA*

²⁰ *Dept. of Astronomy, Ohio State University, Columbus, OH 43210, USA*

²¹ *Dept. of Physics and Center for Cosmology and Astro-Particle Physics, Ohio State University, Columbus, OH 43210, USA*

²² *Niels Bohr Institute, University of Copenhagen, DK-2100 Copenhagen, Denmark*

²³ *Dept. of Physics, TU Dortmund University, D-44221 Dortmund, Germany*

²⁴ *Dept. of Physics and Astronomy, Michigan State University, East Lansing, MI 48824, USA*

²⁵ *Dept. of Physics, University of Alberta, Edmonton, Alberta, Canada T6G 2E1*

²⁶ *Erlangen Centre for Astroparticle Physics, Friedrich-Alexander-Universität Erlangen-Nürnberg, D-91058 Erlangen, Germany*

²⁷ *Physik-department, Technische Universität München, D-85748 Garching, Germany*

²⁸ *Département de physique nucléaire et corpusculaire, Université de Genève, CH-1211 Genève, Switzerland*

²⁹ *Dept. of Physics and Astronomy, University of Gent, B-9000 Gent, Belgium*

- ³⁰ *Dept. of Physics and Astronomy, University of California, Irvine, CA 92697, USA*
- ³¹ *Karlsruhe Institute of Technology, Institute for Astroparticle Physics, D-76021 Karlsruhe, Germany*
- ³² *Karlsruhe Institute of Technology, Institute of Experimental Particle Physics, D-76021 Karlsruhe, Germany*
- ³³ *Dept. of Physics, Engineering Physics, and Astronomy, Queen's University, Kingston, ON K7L 3N6, Canada*
- ³⁴ *Dept. of Physics and Astronomy, University of Kansas, Lawrence, KS 66045, USA*
- ³⁵ *Department of Physics and Astronomy, UCLA, Los Angeles, CA 90095, USA*
- ³⁶ *Centre for Cosmology, Particle Physics and Phenomenology - CP3, Université catholique de Louvain, Louvain-la-Neuve, Belgium*
- ³⁷ *Department of Physics, Mercer University, Macon, GA 31207-0001, USA*
- ³⁸ *Dept. of Astronomy, University of Wisconsin–Madison, Madison, WI 53706, USA*
- ³⁹ *Dept. of Physics and Wisconsin IceCube Particle Astrophysics Center, University of Wisconsin–Madison, Madison, WI 53706, USA*
- ⁴⁰ *Institute of Physics, University of Mainz, Staudinger Weg 7, D-55099 Mainz, Germany*
- ⁴¹ *Department of Physics, Marquette University, Milwaukee, WI, 53201, USA*
- ⁴² *Institut für Kernphysik, Westfälische Wilhelms-Universität Münster, D-48149 Münster, Germany*
- ⁴³ *Bartol Research Institute and Dept. of Physics and Astronomy, University of Delaware, Newark, DE 19716, USA*
- ⁴⁴ *Dept. of Physics, Yale University, New Haven, CT 06520, USA*
- ⁴⁵ *Dept. of Physics, University of Oxford, Parks Road, Oxford OX1 3PU, UK*
- ⁴⁶ *Dept. of Physics, Drexel University, 3141 Chestnut Street, Philadelphia, PA 19104, USA*
- ⁴⁷ *Physics Department, South Dakota School of Mines and Technology, Rapid City, SD 57701, USA*
- ⁴⁸ *Dept. of Physics, University of Wisconsin, River Falls, WI 54022, USA*
- ⁴⁹ *Dept. of Physics and Astronomy, University of Rochester, Rochester, NY 14627, USA*
- ⁵⁰ *Department of Physics and Astronomy, University of Utah, Salt Lake City, UT 84112, USA*
- ⁵¹ *Oskar Klein Centre and Dept. of Physics, Stockholm University, SE-10691 Stockholm, Sweden*
- ⁵² *Dept. of Physics and Astronomy, Stony Brook University, Stony Brook, NY 11794-3800, USA*
- ⁵³ *Dept. of Physics, Sungkyunkwan University, Suwon 16419, Korea*
- ⁵⁴ *Institute of Basic Science, Sungkyunkwan University, Suwon 16419, Korea*
- ⁵⁵ *Institute of Physics, Academia Sinica, Taipei, 11529, Taiwan*
- ⁵⁶ *Dept. of Physics and Astronomy, University of Alabama, Tuscaloosa, AL 35487, USA*
- ⁵⁷ *Dept. of Astronomy and Astrophysics, Pennsylvania State University, University Park, PA 16802, USA*
- ⁵⁸ *Dept. of Physics, Pennsylvania State University, University Park, PA 16802, USA*
- ⁵⁹ *Dept. of Physics and Astronomy, Uppsala University, Box 516, S-75120 Uppsala, Sweden*
- ⁶⁰ *Dept. of Physics, University of Wuppertal, D-42119 Wuppertal, Germany*
- ⁶¹ *DESY, D-15738 Zeuthen, Germany*
- ⁶² *Università di Padova, I-35131 Padova, Italy*
- ⁶³ *National Research Nuclear University, Moscow Engineering Physics Institute (MEPhI), Moscow 115409, Russia*
- ⁶⁴ *Earthquake Research Institute, University of Tokyo, Bunkyo, Tokyo 113-0032, Japan*

The Pierre Auger Collaboration

P. Abreu⁷², M. Aglietta^{54,52}, J.M. Albury¹³, I. Allekotte¹, K. Almeida Cheminant⁷⁰, A. Almela^{8,12}, J. Alvarez-Muñiz⁷⁹, R. Alves Batista⁸⁰, G.A. Anastasi^{54,52}, L. Anchordoqui⁸⁷, B. Andrada⁸, S. Andringa⁷², C. Aramo⁵⁰, P.R. Araújo Ferreira⁴², E. Arnone^{63,52}, J. C. Arteaga Velázquez⁶⁷, H. Asorey⁸, P. Assis⁷², G. Avila¹¹, A.M. Badescu⁷⁵, A. Bakalova³², A. Balaceanu⁷³, F. Barbato^{45,46}, J.A. Bellido^{13,69}, C. Berat³⁶, M.E. Bertaina^{63,52}, X. Bertou¹, G. Bhatta⁷⁰, P.L. Biermann^b,

V. Binet⁶, K. Bismark^{39,8}, T. Bister⁴², J. Biteau³⁷, J. Blazek³², C. Bleve³⁶, J. Blümer⁴¹, M. Boháčová³², D. Boncioli^{57,46}, C. Bonifazi^{9,26}, L. Bonneau Arbeletche²², N. Borodai⁷⁰, A.M. Botti⁸, J. Brack^d, T. Bretz⁴², P.G. Brichetto Orchera⁸, F.L. Briechele⁴², P. Buchholz⁴⁴, A. Bueno⁷⁸, S. Buitink¹⁵, M. Buscemi⁴⁷, M. Büsken^{39,8}, K.S. Caballero-Mora⁶⁶, L. Caccianiga^{59,49}, F. Canfora^{80,81}, I. Caracas³⁸, R. Caruso^{58,47}, A. Castellina^{54,52}, F. Catalani¹⁹, G. Cataldi⁴⁸, L. Cazon⁷², M. Cerda¹⁰, J.A. Chinellato²², J. Chudoba³², L. Chytka³³, R.W. Clay¹³, A.C. Cobos Cerutti⁷, R. Colalillo^{60,50}, A. Coleman⁹³, M.R. Coluccia⁴⁸, R. Conceição⁷², A. Condorelli^{45,46}, G. Consolati^{49,55}, F. Contreras¹¹, F. Convenga⁴¹, D. Correia dos Santos²⁸, C.E. Covault⁸⁵, S. Dasso^{5,3}, K. Daumiller⁴¹, B.R. Dawson¹³, J.A. Day¹³, R.M. de Almeida²⁸, J. de Jesús^{8,41}, S.J. de Jong^{80,81}, J.R.T. de Mello Neto^{26,27}, I. De Mitri^{45,46}, J. de Oliveira¹⁸, D. de Oliveira Franco²², F. de Palma^{56,48}, V. de Souza²⁰, E. De Vito^{56,48}, M. del Río¹¹, O. Deligny³⁴, L. Deval^{41,8}, A. di Matteo⁵², M. Dobre⁷³, C. Dobrigkeit²², J.C. D'Olivo⁶⁸, L.M. Domingues Mendes⁷², R.C. dos Anjos²⁵, M.T. Dova⁴, J. Ebr³², R. Engel^{39,41}, I. Epicoco^{56,48}, M. Erdmann⁴², C.O. Escobar^a, A. Etchegoyen^{8,12}, H. Falcke^{80,82,81}, J. Farmer⁹², G. Farrar⁹⁰, A.C. Fauth²², N. Fazzini^a, F. Feldbusch⁴⁰, F. Fenu^{63,52}, B. Fick⁸⁹, J.M. Figueira⁸, A. Filipčič^{77,76}, T. Fitoussi⁴¹, T. Fodran⁸⁰, T. Fujii^{92,e}, A. Fuster^{8,12}, C. Galea⁸⁰, C. Galelli^{59,49}, B. García⁷, A.L. Garcia Vegas⁴², H. Gemmeke⁴⁰, F. Gesualdi^{8,41}, A. Gherghel-Lascu⁷³, P.L. Ghia³⁴, U. Giaccari⁸⁰, M. Giammarchi⁴⁹, J. Glombitza⁴², F. Gobbi¹⁰, F. Gollan⁸, G. Golup¹, M. Gómez Berisso¹, P.F. Gómez Vitale¹¹, J.P. Gongora¹¹, J.M. González¹, N. González¹⁴, I. Goos^{1,41}, D. Góra⁷⁰, A. Gorgi^{54,52}, M. Gottowik³⁸, T.D. Grubb¹³, F. Guarino^{60,50}, G.P. Guedes²³, E. Guido^{52,63}, S. Hahn^{41,8}, P. Hamal³², M.R. Hampel⁸, P. Hansen⁴, D. Harari¹, V.M. Harvey¹³, T. Hebbeker⁴², D. Heck⁴¹, C. Hojvat^a, J.R. Hörandel^{80,81}, P. Horvath³³, M. Hrabovský³³, T. Huege^{41,15}, A. Insolia^{58,47}, P.G. Isar⁷⁴, P. Janecek³², J.A. Johnsen⁸⁶, J. Jurysek³², A. Kääpä³⁸, K.H. Kampert³⁸, N. Karastathis⁴¹, B. Keilhauer⁴¹, J. Kemp⁴², A. Khakurdikar⁸⁰, V.V. Kizakke Covilakam^{8,41}, H.O. Klages⁴¹, M. Kleifges⁴⁰, J. Kleinfeller¹⁰, F. Knapp³⁹, N. Kunka⁴⁰, B.L. Lago¹⁷, R.G. Lang²⁰, N. Langner⁴², M.A. Leigui de Oliveira²⁴, V. Lenok⁴¹, A. Letessier-Selvon³⁵, I. Lhenry-Yvon³⁴, D. Lo Presti^{58,47}, L. Lopes⁷², R. López⁶⁴, L. Lu⁹⁴, Q. Luce³⁹, J.P. Lundquist⁷⁶, A. Machado Payeras²², G. Mancarella^{56,48}, D. Mandat³², B.C. Manning¹³, J. Manshanden⁴³, P. Mantsch^a, S. Marafico³⁴, F.M. Mariani^{59,49}, A.G. Mariazzi⁴, I.C. Mariş¹⁴, G. Marsella^{61,47}, D. Martello^{56,48}, S. Martinelli^{41,8}, O. Martínez Bravo⁶⁴, M. Mastrodicasa^{57,46}, H.J. Mathes⁴¹, J. Matthews⁸⁸, G. Matthiae^{62,51}, E. Mayotte^{86,38}, S. Mayotte³⁸, P.O. Mazur^a, G. Medina-Tanco⁶⁸, D. Melo⁸, A. Menshikov⁴⁰, S. Michal³³, M.I. Micheletti⁶, L. Miramonti^{59,49}, S. Mollerach¹, F. Montanet³⁶, L. Morejon³⁸, C. Morello^{54,52}, M. Mostafá⁹¹, A.L. Müller³², M.A. Muller²², K. Mulrey^{80,81}, R. Mussa⁵², M. Muzio⁹⁰, W.M. Namasaka³⁸, A. Nasr-Esfahani³⁸, L. Nellen⁶⁸, G. Nicora², M. Niculescu-Oglinزانu⁷³, M. Niechciol⁴⁴, D. Nitz⁸⁹, D. Nosek³¹, V. Novotny³¹, L. Nožka³³, A. Nucita^{56,48}, L.A. Núñez³⁰, C. Oliveira²⁰, M. Palatka³², J. Pallotta², P. Papenbreer³⁸, G. Parente⁷⁹, A. Parra⁶⁴, J. Pawlowsky³⁸, M. Pech³², F. Pedreira⁷⁹, J. Peřkala⁷⁰, R. Pelayo⁶⁵, J. Peña-Rodríguez³⁰, E.E. Pereira Martins^{39,8}, J. Perez Armand²¹, C. Pérez Bertolli^{8,41}, M. Perlin^{8,41}, L. Perrone^{56,48}, S. Petrera^{45,46}, T. Pierog⁴¹, M. Pimenta⁷², V. Pirronello^{58,47}, M. Platino⁸, B. Pont⁸⁰, M. Pothast^{81,80}, P. Privitera⁹², M. Prouza³², A. Puyleart⁸⁹, S. Querchfeld³⁸, J. Rautenberg³⁸, D. Ravignani⁸, M. Reininghaus^{41,8}, J. Ridky³², F. Riehn⁷², M. Risse⁴⁴, V. Rizi^{57,46}, W. Rodrigues de Carvalho⁸⁰, J. Rodriguez Rojo¹¹, M.J. Roncoroni⁸, S. Rossoni⁴³, M. Roth⁴¹, E. Roulet¹, A.C. Rovero⁵, P. Ruehl⁴⁴, A. Saftoiu⁷³, M. Saharan⁸⁰, F. Salamida^{57,46}, H. Salazar⁶⁴, G. Salina⁵¹, J.D. Sanabria Gomez³⁰, F. Sánchez⁸, E.M. Santos²¹, E. Santos³², F. Sarazin⁸⁶, R. Sarmiento⁷², C. Sarmiento-Cano⁸, R. Sato¹¹, P. Savina⁹⁴,

C.M. Schäfer⁴¹, V. Scherini^{56,48}, H. Schieler⁴¹, M. Schimassek^{39,8}, M. Schimp³⁸, F. Schlüter^{41,8}, D. Schmidt³⁹, O. Scholten^{84,15}, H. Schoorlemmer^{80,81}, P. Schovánek³², J. Schulte⁴², T. Schulz⁴¹, S.J. Sciutto⁴, M. Scornavacche^{8,41}, A. Segreto^{53,47}, S. Sehgal³⁸, R.C. Shellard¹⁶, G. Sigl⁴³, G. Silli^{8,41}, O. Sima^{73,f}, R. Smau⁷³, R. Šmída⁹², P. Sommers⁹¹, J.F. Soriano⁸⁷, R. Squartini¹⁰, M. Stadelmaier^{41,8}, D. Stanca⁷³, S. Stanič⁷⁶, J. Stasielak⁷⁰, P. Stassi³⁶, A. Streich^{39,8}, M. Suárez-Durán¹⁴, T. Sudholz¹³, T. Suomijärvi³⁷, A.D. Supanitsky⁸, Z. Szadkowski⁷¹, A. Tapia²⁹, C. Taricco^{63,52}, C. Timmermans^{81,80}, O. Tkachenko⁴¹, P. Tobiska³², C.J. Todero Peixoto¹⁹, B. Tomé⁷², Z. Torrès³⁶, A. Travaini¹⁰, P. Travnicek³², C. Trimarelli^{57,46}, M. Tueros⁴, R. Ulrich⁴¹, M. Unger⁴¹, L. Vaclavek³³, M. Vacula³³, J.F. Valdés Galicia⁶⁸, L. Valore^{60,50}, E. Varela⁶⁴, A. Vásquez-Ramírez³⁰, D. Veberič⁴¹, C. Ventura²⁷, I.D. Vergara Quispe⁴, V. Verzi⁵¹, J. Vicha³², J. Vink⁸³, S. Vorobiov⁷⁶, H. Wahlberg⁴, C. Watanabe²⁶, A.A. Watson^c, L. Wiencke⁸⁶, H. Wilczyński⁷⁰, M. Wirtz⁴², D. Wittkowski³⁸, B. Wundheiler⁸, A. Yushkov³², O. Zapparrata¹⁴, E. Zas⁷⁹, D. Zavrtnik^{76,77}, M. Zavrtnik^{77,76}, L. Zehrer⁷⁶

¹ *Centro Atómico Bariloche and Instituto Balseiro (CNEA-UNCuyo-CONICET), San Carlos de Bariloche, Argentina*

² *Centro de Investigaciones en Láseres y Aplicaciones, CITEDEF and CONICET, Villa Martelli, Argentina*

³ *Departamento de Física and Departamento de Ciencias de la Atmósfera y los Océanos, FCEyN, Universidad de Buenos Aires and CONICET, Buenos Aires, Argentina*

⁴ *IFLP, Universidad Nacional de La Plata and CONICET, La Plata, Argentina*

⁵ *Instituto de Astronomía y Física del Espacio (IAFE, CONICET-UBA), Buenos Aires, Argentina*

⁶ *Instituto de Física de Rosario (IFIR) – CONICET/U.N.R. and Facultad de Ciencias Bioquímicas y Farmacéuticas U.N.R., Rosario, Argentina*

⁷ *Instituto de Tecnologías en Detección y Astropartículas (CNEA, CONICET, UNSAM), and Universidad Tecnológica Nacional – Facultad Regional Mendoza (CONICET/CNEA), Mendoza, Argentina*

⁸ *Instituto de Tecnologías en Detección y Astropartículas (CNEA, CONICET, UNSAM), Buenos Aires, Argentina*

⁹ *International Center of Advanced Studies and Instituto de Ciencias Físicas, ECyT-UNSAM and CONICET, Campus Miguelete – San Martín, Buenos Aires, Argentina*

¹⁰ *Observatorio Pierre Auger, Malargüe, Argentina*

¹¹ *Observatorio Pierre Auger and Comisión Nacional de Energía Atómica, Malargüe, Argentina*

¹² *Universidad Tecnológica Nacional – Facultad Regional Buenos Aires, Buenos Aires, Argentina*

¹³ *University of Adelaide, Adelaide, S.A., Australia*

¹⁴ *Université Libre de Bruxelles (ULB), Brussels, Belgium*

¹⁵ *Vrije Universiteit Brussels, Brussels, Belgium*

¹⁶ *Centro Brasileiro de Pesquisas Físicas, Rio de Janeiro, RJ, Brazil*

¹⁷ *Centro Federal de Educação Tecnológica Celso Suckow da Fonseca, Nova Friburgo, Brazil*

¹⁸ *Instituto Federal de Educação, Ciência e Tecnologia do Rio de Janeiro (IFRJ), Brazil*

¹⁹ *Universidade de São Paulo, Escola de Engenharia de Lorena, Lorena, SP, Brazil*

²⁰ *Universidade de São Paulo, Instituto de Física de São Carlos, São Carlos, SP, Brazil*

²¹ *Universidade de São Paulo, Instituto de Física, São Paulo, SP, Brazil*

²² *Universidade Estadual de Campinas, IFGW, Campinas, SP, Brazil*

²³ *Universidade Estadual de Feira de Santana, Feira de Santana, Brazil*

²⁴ *Universidade Federal do ABC, Santo André, SP, Brazil*

²⁵ *Universidade Federal do Paraná, Setor Palotina, Palotina, Brazil*

²⁶ *Universidade Federal do Rio de Janeiro, Instituto de Física, Rio de Janeiro, RJ, Brazil*

²⁷ *Universidade Federal do Rio de Janeiro (UFRJ), Observatório do Valongo, Rio de Janeiro, RJ, Brazil*

- ²⁸ *Universidade Federal Fluminense, EEIMVR, Volta Redonda, RJ, Brazil*
- ²⁹ *Universidad de Medellín, Medellín, Colombia*
- ³⁰ *Universidad Industrial de Santander, Bucaramanga, Colombia*
- ³¹ *Charles University, Faculty of Mathematics and Physics, Institute of Particle and Nuclear Physics, Prague, Czech Republic*
- ³² *Institute of Physics of the Czech Academy of Sciences, Prague, Czech Republic*
- ³³ *Palacky University, RCPTM, Olomouc, Czech Republic*
- ³⁴ *CNRS/IN2P3, IJCLab, Université Paris-Saclay, Orsay, France*
- ³⁵ *Laboratoire de Physique Nucléaire et de Hautes Energies (LPNHE), Sorbonne Université, Université de Paris, CNRS-IN2P3, Paris, France*
- ³⁶ *Univ. Grenoble Alpes, CNRS, Grenoble Institute of Engineering Univ. Grenoble Alpes, LPSC-IN2P3, 38000 Grenoble, France*
- ³⁷ *Université Paris-Saclay, CNRS/IN2P3, IJCLab, Orsay, France*
- ³⁸ *Bergische Universität Wuppertal, Department of Physics, Wuppertal, Germany*
- ³⁹ *Karlsruhe Institute of Technology (KIT), Institute for Experimental Particle Physics, Karlsruhe, Germany*
- ⁴⁰ *Karlsruhe Institute of Technology (KIT), Institut für Prozessdatenverarbeitung und Elektronik, Karlsruhe, Germany*
- ⁴¹ *Karlsruhe Institute of Technology (KIT), Institute for Astroparticle Physics, Karlsruhe, Germany*
- ⁴² *RWTH Aachen University, III. Physikalisches Institut A, Aachen, Germany*
- ⁴³ *Universität Hamburg, II. Institut für Theoretische Physik, Hamburg, Germany*
- ⁴⁴ *Universität Siegen, Department Physik – Experimentelle Teilchenphysik, Siegen, Germany*
- ⁴⁵ *Gran Sasso Science Institute, L’Aquila, Italy*
- ⁴⁶ *INFN Laboratori Nazionali del Gran Sasso, Assergi (L’Aquila), Italy*
- ⁴⁷ *INFN, Sezione di Catania, Catania, Italy*
- ⁴⁸ *INFN, Sezione di Lecce, Lecce, Italy*
- ⁴⁹ *INFN, Sezione di Milano, Milano, Italy*
- ⁵⁰ *INFN, Sezione di Napoli, Napoli, Italy*
- ⁵¹ *INFN, Sezione di Roma “Tor Vergata”, Roma, Italy*
- ⁵² *INFN, Sezione di Torino, Torino, Italy*
- ⁵³ *Istituto di Astrofisica Spaziale e Fisica Cosmica di Palermo (INAF), Palermo, Italy*
- ⁵⁴ *Osservatorio Astrofisico di Torino (INAF), Torino, Italy*
- ⁵⁵ *Politecnico di Milano, Dipartimento di Scienze e Tecnologie Aerospaziali, Milano, Italy*
- ⁵⁶ *Università del Salento, Dipartimento di Matematica e Fisica “E. De Giorgi”, Lecce, Italy*
- ⁵⁷ *Università dell’Aquila, Dipartimento di Scienze Fisiche e Chimiche, L’Aquila, Italy*
- ⁵⁸ *Università di Catania, Dipartimento di Fisica e Astronomia “Ettore Majorana”, Catania, Italy*
- ⁵⁹ *Università di Milano, Dipartimento di Fisica, Milano, Italy*
- ⁶⁰ *Università di Napoli “Federico II”, Dipartimento di Fisica “Ettore Pancini”, Napoli, Italy*
- ⁶¹ *Università di Palermo, Dipartimento di Fisica e Chimica “E. Segrè”, Palermo, Italy*
- ⁶² *Università di Roma “Tor Vergata”, Dipartimento di Fisica, Roma, Italy*
- ⁶³ *Università Torino, Dipartimento di Fisica, Torino, Italy*
- ⁶⁴ *Benemérita Universidad Autónoma de Puebla, Puebla, México*
- ⁶⁵ *Unidad Profesional Interdisciplinaria en Ingeniería y Tecnologías Avanzadas del Instituto Politécnico Nacional (UPIITA-IPN), México, D.F., México*
- ⁶⁶ *Universidad Autónoma de Chiapas, Tuxtla Gutiérrez, Chiapas, México*

- ⁶⁷ *Universidad Michoacana de San Nicolás de Hidalgo, Morelia, Michoacán, México*
- ⁶⁸ *Universidad Nacional Autónoma de México, México, D.F., México*
- ⁶⁹ *Universidad Nacional de San Agustín de Arequipa, Facultad de Ciencias Naturales y Formales, Arequipa, Peru*
- ⁷⁰ *Institute of Nuclear Physics PAN, Krakow, Poland*
- ⁷¹ *University of Łódź, Faculty of High-Energy Astrophysics, Łódź, Poland*
- ⁷² *Laboratório de Instrumentação e Física Experimental de Partículas – LIP and Instituto Superior Técnico – IST, Universidade de Lisboa – UL, Lisboa, Portugal*
- ⁷³ *“Horia Hulubei” National Institute for Physics and Nuclear Engineering, Bucharest-Magurele, Romania*
- ⁷⁴ *Institute of Space Science, Bucharest-Magurele, Romania*
- ⁷⁵ *University Politehnica of Bucharest, Bucharest, Romania*
- ⁷⁶ *Center for Astrophysics and Cosmology (CAC), University of Nova Gorica, Nova Gorica, Slovenia*
- ⁷⁷ *Experimental Particle Physics Department, J. Stefan Institute, Ljubljana, Slovenia*
- ⁷⁸ *Universidad de Granada and C.A.F.P.E., Granada, Spain*
- ⁷⁹ *Instituto Galego de Física de Altas Enerxías (IGFAE), Universidade de Santiago de Compostela, Santiago de Compostela, Spain*
- ⁸⁰ *IMAPP, Radboud University Nijmegen, Nijmegen, The Netherlands*
- ⁸¹ *Nationaal Instituut voor Kernfysica en Hoge Energie Fysica (NIKHEF), Science Park, Amsterdam, The Netherlands*
- ⁸² *Stichting Astronomisch Onderzoek in Nederland (ASTRON), Dwingeloo, The Netherlands*
- ⁸³ *Universiteit van Amsterdam, Faculty of Science, Amsterdam, The Netherlands*
- ⁸⁴ *University of Groningen, Kapteyn Astronomical Institute, Groningen, The Netherlands*
- ⁸⁵ *Case Western Reserve University, Cleveland, OH, USA*
- ⁸⁶ *Colorado School of Mines, Golden, CO, USA*
- ⁸⁷ *Department of Physics and Astronomy, Lehman College, City University of New York, Bronx, NY, USA*
- ⁸⁸ *Louisiana State University, Baton Rouge, LA, USA*
- ⁸⁹ *Michigan Technological University, Houghton, MI, USA*
- ⁹⁰ *New York University, New York, NY, USA*
- ⁹¹ *Pennsylvania State University, University Park, PA, USA*
- ⁹² *University of Chicago, Enrico Fermi Institute, Chicago, IL, USA*
- ⁹³ *University of Delaware, Department of Physics and Astronomy, Bartol Research Institute, Newark, DE, USA*
- ⁹⁴ *University of Wisconsin-Madison, Department of Physics and WIPAC, Madison, WI, USA*
-
- ^a *Fermi National Accelerator Laboratory, Fermilab, Batavia, IL, USA*
- ^b *Max-Planck-Institut für Radioastronomie, Bonn, Germany*
- ^c *School of Physics and Astronomy, University of Leeds, Leeds, United Kingdom*
- ^d *Colorado State University, Fort Collins, CO, USA*
- ^e *now at Hakubi Center for Advanced Research and Graduate School of Science, Kyoto University, Kyoto, Japan*
- ^f *also at University of Bucharest, Physics Department, Bucharest, Romania*

The Telescope Array Collaboration

T. Abu-Zayyad^{1,2}, M. Allen², Y. Arai³, R. Arimura³, E. Barcikowski², J.W. Belz², D.R. Bergman², S.A. Blake², I. Buckland², R. Cady², B.G. Cheon⁴, J. Chiba⁵, M. Chikawa⁶, K. Fujisue⁶, K. Fujita³, R. Fujiwara³, M. Fukushima⁶, R. Fukushima³, G. Furlich², N. Globus^{8,a}, R. Gonzalez², W. Hanlon², M. Hayashi⁹, N. Hayashida¹⁰, H. He⁸, K. Hibino¹⁰, R. Higuchi⁶, K. Honda¹¹, D. Ikeda¹⁰, T. Inadomi⁹,

N. Inoue¹², T. Ishii¹¹, H. Ito⁸, D. Ivanov², H. Iwakura⁹, A. Iwasaki³, H.M. Jeong¹³, S. Jeong¹³, C.C.H. Jui², K. Kadota¹⁴, F. Kakimoto¹⁰, O. Kalashev¹⁵, K. Kasahara¹⁶, S. Kasami¹⁷, S. Kawakami³, S. Kawana¹², K. Kawata⁶, I. Kharuk¹⁵, E. Kido⁸, H.B. Kim⁴, J.H. Kim², J.H. Kim², S.W. Kim¹³, Y. Kimura³, S. Kishigami³, Y. Kubota⁹, S. Kurisu⁹, V. Kuzmin^{15,b}, M. Kuznetsov^{15,18}, Y.J. Kwon¹⁹, K.H. Lee¹³, B. Lubsandorzhiev¹⁵, K. Machida¹¹, H. Matsumiya³, T. Matsuyama³, J.N. Matthews², R. Mayta³, M. Minamino³, K. Mukai¹¹, I. Myers², S. Nagataki⁸, K. Nakai³, R. Nakamura⁹, T. Nakamura²¹, T. Nakamura⁹, Y. Nakamura⁹, A. Nakazawa⁹, E. Nishio¹⁷, T. Nonaka⁶, H. Oda³, S. Ogio^{3,22}, M. Ohnishi⁶, H. Ohoka⁶, Y. Oku¹⁷, T. Okuda²³, Y. Omura³, M. Ono⁸, R. Onogi³, A. Oshima²⁴, S. Ozawa²⁵, I.H. Park¹³, M. Potts², M.S. Pshirkov^{15,26}, J. Remington², D.C. Rodriguez², G.I. Rubtsov¹⁵, D. Ryu²⁷, H. Sagawa⁶, R. Sahara³, Y. Saito⁹, N. Sakaki⁶, T. Sako⁶, N. Sakurai³, K. Sano⁹, K. Sato³, T. Seki⁹, K. Sekino⁶, P.D. Shah², Y. Shibasaki⁹, F. Shibata¹¹, N. Shibata¹⁷, T. Shibata⁶, H. Shimodaira⁶, B.K. Shin²⁷, H.S. Shin⁶, D. Shinto¹⁷, J.D. Smith², P. Sokolsky², N. Sone⁹, B.T. Stokes², T.A. Stroman², Y. Takagi³, Y. Takahashi³, M. Takamura⁵, M. Takeda⁶, R. Takeishi⁶, A. Taketa²⁸, M. Takita⁶, Y. Tameda¹⁷, H. Tanaka³, K. Tanaka²⁹, M. Tanaka³⁰, Y. Tanoue³, S.B. Thomas², G.B. Thomson², P. Tinyakov^{15,18}, I. Tkachev¹⁵, H. Tokuno³¹, T. Tomida⁹, S. Troitsky¹⁵, R. Tsuda³, Y. Tsunesada^{3,22}, Y. Uchihori³², S. Udo¹⁰, T. Uehama⁹, F. Urban³³, D. Warren⁸, T. Wong², M. Yamamoto⁹, K. Yamazaki²⁴, K. Yashiro⁵, F. Yoshida¹⁷, Y. Yoshioka⁹, Y. Zhezher^{6,15}, and Z. Zundel²

¹ *Department of Physics, Loyola University Chicago, Chicago, Illinois, USA*

² *High Energy Astrophysics Institute and Department of Physics and Astronomy, University of Utah, Salt Lake City, Utah, USA*

³ *Graduate School of Science, Osaka City University, Osaka, Osaka, Japan*

⁴ *Department of Physics and The Research Institute of Natural Science, Hanyang University, Seongdong-gu, Seoul, Korea*

⁵ *Department of Physics, Tokyo University of Science, Noda, Chiba, Japan*

⁶ *Institute for Cosmic Ray Research, University of Tokyo, Kashiwa, Chiba, Japan*

⁷ *The Hakubi Center for Advanced Research and Graduate School of Science, Kyoto University, Kitashirakawa-Oiwakecho, Sakyo-ku, Kyoto, Japan*

⁸ *Astrophysical Big Bang Laboratory, RIKEN, Wako, Saitama, Japan*

⁹ *Academic Assembly School of Science and Technology Institute of Engineering, Shinshu University, Nagano, Nagano, Japan*

¹⁰ *Faculty of Engineering, Kanagawa University, Yokohama, Kanagawa, Japan*

¹¹ *Interdisciplinary Graduate School of Medicine and Engineering, University of Yamanashi, Kofu, Yamanashi, Japan*

¹² *The Graduate School of Science and Engineering, Saitama University, Saitama, Saitama, Japan*

¹³ *Department of Physics, SungKyunKwan University, Jang-an-gu, Suwon, Korea*

¹⁴ *Department of Physics, Tokyo City University, Setagaya-ku, Tokyo, Japan*

¹⁵ *Institute for Nuclear Research of the Russian Academy of Sciences, Moscow, Russia*

¹⁶ *Faculty of Systems Engineering and Science, Shibaura Institute of Technology, Minato-ku, Tokyo, Japan*

¹⁷ *Department of Engineering Science, Faculty of Engineering, Osaka Electro-Communication University, Neyagawa-shi, Osaka, Japan*

¹⁸ *Service de Physique Théorique, Université Libre de Bruxelles, Brussels, Belgium*

¹⁹ *Department of Physics, Yonsei University, Seodaemun-gu, Seoul, Korea*

²⁰ *Center for Astrophysics and Cosmology, University of Nova Gorica, Nova Gorica, Slovenia*

²¹ *Faculty of Science, Kochi University, Kochi, Kochi, Japan*

²² *Nambu Yoichiro Institute of Theoretical and Experimental Physics, Osaka City University, Osaka, Osaka, Japan*

²³ *Department of Physical Sciences, Ritsumeikan University, Kusatsu, Shiga, Japan*

²⁴ *College of Engineering, Chubu University, Kasugai, Aichi, Japan*

²⁵ *Quantum ICT Advanced Development Center, National Institute for Information and Communications Technology, Koganei, Tokyo, Japan*

²⁶ *Sternberg Astronomical Institute, Moscow M.V. Lomonosov State University, Moscow, Russia*

²⁷ *Department of Physics, School of Natural Sciences, Ulsan National Institute of Science and Technology, UNIST-gil, Ulsan, Korea*

²⁸ *Earthquake Research Institute, University of Tokyo, Bunkyo-ku, Tokyo, Japan*

²⁹ *Graduate School of Information Sciences, Hiroshima City University, Hiroshima, Hiroshima, Japan*

³⁰ *Institute of Particle and Nuclear Studies, KEK, Tsukuba, Ibaraki, Japan*

³¹ *Graduate School of Science and Engineering, Tokyo Institute of Technology, Meguro, Tokyo, Japan*

³² *Department of Research Planning and Promotion, Quantum Medical Science Directorate, National Institutes for Quantum and Radiological Science and Technology, Chiba, Chiba, Japan*

³³ *CEICO, Institute of Physics, Czech Academy of Sciences, Prague, Czech Republic*

—

^a *Presently at: University of California - Santa Cruz and Flatiron Institute, Simons Foundation*

^b *Deceased*

Search for Spatial Correlations of Neutrinos with Ultra-High-Energy Cosmic Rays

(Received receipt date; Revised revision date; Accepted acceptance date; Published published date)

Submitted to Astrophysical Journal

ABSTRACT

1 For several decades, the origin of ultra-high-energy cosmic rays (UHECRs) has been
2 an unsolved question of high-energy astrophysics. One approach for solving this puzzle
3 is to correlate UHECRs with high-energy neutrinos, since neutrinos are a direct probe
4 of hadronic interactions of cosmic rays and are not deflected by magnetic fields. In
5 this paper, we present three different approaches for correlating the arrival directions of
6 neutrinos with the arrival directions of UHECRs. The neutrino data is provided by the
7 IceCube Neutrino Observatory and ANTARES, while the UHECR data with energies
8 above ~ 50 EeV is provided by the Pierre Auger Observatory and the Telescope Array.
9 All experiments provide increased statistics and improved reconstructions with respect
10 to our previous results reported in 2015. The first analysis uses a high-statistics neutrino
11 sample optimized for point-source searches to search for excesses of neutrinos clustering
12 in the vicinity of UHECR directions. The second analysis searches for an excess of
13 UHECRs in the direction of the highest-energy neutrinos. The third analysis searches
14 for an excess of pairs of UHECRs and highest-energy neutrinos on different angular
15 scales. None of the analyses has found a significant excess, and previously reported over-
16 fluctuations are reduced in significance. Based on these results, we further constrain
17 the neutrino flux spatially correlated with UHECRs.

Keywords: Neutrino astronomy; Ultra-high-energy cosmic radiation; tbd.

Contents

1. Introduction	13
2. Observatories and data sets	15
2.1. The IceCube Neutrino Observatory	15
2.2. The ANTARES Neutrino Telescope	17
2.3. The Pierre Auger Observatory	19
2.4. The Telescope Array	19
3. Magnetic deflections	20
4. Analysis methods	21
4.1. Unbinned neutrino point-source search with UHECR information	21

4.2. Unbinned likelihood-stacking analysis of UHECRs and high-energy neutrinos	26
4.3. Two-point angular correlation of UHECRs and high-energy neutrinos	28
5. Results	28
5.1. Unbinned neutrino point-source search with UHECR information	28
5.2. Unbinned likelihood-stacking analysis of UHECRs and high-energy neutrinos	29
5.3. Two-point angular correlation of UHECRs and high-energy neutrinos	30
6. Conclusions	30

1. INTRODUCTION

The Earth is continuously bombarded by high-energy cosmic rays, most of which are charged atomic nuclei (Particle Data Group et al. 2020). It is generally believed that cosmic rays with energies above 1 EeV (10^{18} eV), known as ultra-high-energy cosmic rays (UHECRs), mostly originate from extragalactic sources in the nearby universe. Based on the estimated magnitude of galactic magnetic fields (Nagano & Watson 2000), cosmic rays below this energy are believed to diffuse within their host galaxy, whereas cosmic rays above this energy escape from the galaxy. These assumptions are confirmed by the observation of large-scale anisotropies in the arrival directions of UHECRs above 8 EeV with the excess flux directed from outside of our Galaxy (Aab et al. 2017). The two largest observatories for UHECRs are the Pierre Auger Observatory (Auger) (The Pierre Auger Collaboration 2015) in Argentina in the Southern hemisphere and Telescope Array (TA) in the United States in the Northern hemisphere (Abu-Zayyad et al. 2012). They have performed detailed analyses of the arrival directions of detected UHECRs and have revealed interesting features, such as possible correlations with the directions of known starburst and active galaxies in the nearby universe observed by Auger (Aab et al. 2018; Abreu et al. 2021), and intermediate-scale directional clustering observed by TA (Abbasi et al. 2014; Tkachev et al. 2021). However, due to the small number of events detected at the highest energies, these indications of anisotropic arrival directions have not yet been confirmed on the 5σ level. Thus, neither Auger nor TA report an unambiguous identification of the UHECR sources to date. One of the main reasons is the deflection of cosmic rays by magnetic fields during propagation from their sources to Earth, which alters their directional information with respect to the source positions. The deflection of UHECRs increases with increasing charge, which is not well determined at the highest energies above 50 EeV considered in this work. This uncertainty additionally complicates the identification of UHECR sources. Nevertheless, UHECRs at the highest energies are deflected the least due to their extremely high magnetic rigidity (Alves Batista et al. 2019), which makes them suitable for directional correlation searches.

We search for the sources of the highest-energy cosmic rays with a multi-messenger approach using high-energy neutrinos and UHECRs with energies above ~ 50 EeV. High-energy neutrinos are direct tracers of hadronic interactions of cosmic rays, and are thus expected to be produced at or near the acceleration sites (see e.g. Murase 2015; Meszaros 2018; Anchordoqui et al. 2008). Furthermore, the electrically-neutral neutrinos carry the directional information of their origin, since they are not deflected by magnetic fields. A combined analysis of UHECRs and high-energy neutrinos is further motivated by the observation of a diffuse flux of high-energy neutrinos of astrophysical origin above the background of atmospheric neutrinos. The flux follows a hard power law that extends to

energies of multiple PeV and possibly beyond (The IceCube Collaboration 2013; Aartsen et al. 2016; Stettner 2019; Aartsen et al. 2020a; Abbasi et al. 2021). The measured flux is closely below the Waxman-Bahcall bound (Waxman & Bahcall 1999; Bahcall & Waxman 2001), which is a theoretical upper bound on the astrophysical neutrino flux derived from the observed UHECR flux, suggesting a connection between UHECRs and high-energy neutrinos (Murase et al. 2013; Ahlers & Halzen 2018). We note that the Seyfert and Starburst Galaxy NGC 1068 appears both as a neutrino source candidate in Aartsen et al. (2020b) and as a UHECR source candidate in Aab et al. (2018). Recently, the potential of high-energy neutrinos in a multi-messenger approach has been demonstrated together with observations of high-energy photons (Aartsen et al. 2018a,b), finding compelling evidence for neutrino emission from the blazar TXS 0506+056. At the same time, it can be concluded that blazars seem insufficient to saturate the total observed neutrino flux (Murase & Waxman 2016; Aartsen et al. 2017a) based on the non-observation of steady neutrino fluxes from known blazars in the universe. This result motivates different approaches to identify hadronic sources in the local universe; a promising method is to correlate the sources traced with UHECRs with high-energy neutrinos, and vice versa.

In this paper, we report results from three conceptually different approaches. All are based on correlating the arrival directions of high-energy neutrinos detected by the IceCube Neutrino Observatory (IC) (Aartsen et al. 2017b) and the ANTARES experiment (ANT) (Ageron et al. 2011) with the arrival directions of UHECRs with energies above ~ 50 EeV measured by Auger and TA:

- Analysis 1 (described in subsection 4.1) uses the measured UHECR directions as well as magnetic deflection estimates for identifying regions in which we search for point-like neutrino sources.
- Analysis 2 (described in subsection 4.2) uses the arrival directions of neutrinos with a high probability of astrophysical origin to search for a correlated clustering of UHECR arrival directions, while also accounting for the magnetic deflection.
- Analysis 3 (described in subsection 4.3) is based on a largely model-independent two-point correlation analysis of the arrival directions of UHECR and neutrinos with a high probability of astrophysical origin.

With these three approaches, we follow up on previous searches performed by the Pierre Auger, Telescope Array and IceCube collaborations (The IceCube Collaboration et al. 2016), which showed an interesting correlation at a significance level close to three standard deviations.

Since 2015, the analyses have been improved with substantially enlarged data sets, extending the Auger data from 10 yr to 13 yr (see subsection 2.3) and TA data from 6 yr to 9 yr (see subsection 2.4). The different data sets from IceCube are enlarged from 4 yr to 10.5 yr, from 4 yr to 7.5 yr, and from 2 yr to 8 yr, depending on the specific detection channel as described in subsection 2.1. Newly included are two data sets of 9 yr and 11 yr from ANTARES, as further specified in subsection 2.2. Due to the updated data sets by Auger and TA, their respective shift of the energy scale is updated from a sole shift of TA energies by -13% to a shift of $+14\%$ for Auger and -14% TA energies above the energy threshold of ~ 50 EeV (Biteau et al. 2019). Furthermore, we include an improved magnetic deflection model that distinguishes between the Northern and Southern hemisphere for analysis 2. We report the results from the three improved correlation searches, which update the preliminary reported results in Schumacher (2019); Aublin et al. (2019); Barbano (2019). In addition, we report

upper limits on the correlated fluxes of UHECRs and neutrinos based on benchmark models for the magnetic deflections.

2. OBSERVATORIES AND DATA SETS

All data sets used in this paper are used in previous work by the four respective collaborations. This section focuses on the main aspects relevant for our analyses.

2.1. *The IceCube Neutrino Observatory*

The IceCube Neutrino Observatory (Aartsen et al. 2017b) is an ice-Cherenkov detector sensitive to neutrinos with energies ≥ 5 GeV. It is located at the geographic South Pole, about 1.45 km to 2.45 km deep in the ice. Its main component consists of a volume of about 1 km^3 glacial ice instrumented with 5160 photo-multipliers which are connected to the surface by 86 cable strings.

Two classes of neutrino-induced events can be phenomenologically distinguished: elongated, track-like events are produced by muons that originate mostly from charged-current ν_μ interactions; and the spherical, cascade-like events that originate from charged-current ν_e and ν_τ interactions with hadronic and electromagnetic decays, as well as neutral-current interactions of all flavors. Typically, track-like events enable a better angular resolution than cascade-like events due to their different topologies, but provide a poorer energy resolution (Aartsen et al. 2014a; Wandkowsky 2018). One method of suppressing the dominant background of down-going muons produced by cosmic-ray interactions in the atmosphere is by selecting events with the interaction vertex within the detector (Aartsen et al. 2014b; Kopper 2017; Wandkowsky 2018). Alternatively, through-going tracks with either horizontal or up-going directions are selected, such that the atmospheric muons are blocked out by Earth (Aartsen et al. 2016; Haack & Wiebusch 2017). In the case of down-going tracks, a high energy threshold together with elaborate selection procedures are necessary to filter out atmospheric muons (Aartsen et al. 2018b, 2017c,d). In all cases, the remaining event rate is dominated by atmospheric neutrinos. The selection of astrophysical neutrinos can be achieved on a statistical basis by selecting very energetic events or, in case of the very down-going region, by vetoing events where an atmospheric shower is observed in IceTop, IceCube’s surface detector for cosmic rays (Abbasi et al. 2013).

For the three analyses, data from multiple detection channels are used, which are: (i) a data set of through-going tracks from the full sky optimized for point-source searches (PS), (ii) a data set of high-energy starting events (HESE) of both topologies from the full sky, (iii) a data set of high-energy neutrinos (HENU) selected from through-going tracks with horizontal and up-going directions, and (iv) a data set of tracks from a selection of extremely high-energy events (EHE). The PS data set is used for analysis 1, while the HESE, HENU and EHE data sets are used for analyses 2 and 3. For analyses 2 and 3, track-like events from the HESE, HENU, and EHE data sets are combined, while multiple instances of identical events are removed. This results in a data set of 81 track-like events. In analyses 2 and 3, the 76 cascade-like events from the HESE data set are analyzed separately due to their larger directional uncertainty. The sky distribution of selected events is shown in Figure 1 and an overview of the nomenclature is presented in Table 1.

The PS data set consists of a combination of data collected from 7 years of operation between 2008 and 2015 that was used for point-source searches (Aartsen et al. 2017d) and data from 3.5 years of operation between 2015 and 2018 that was selected for the real-time gamma-ray follow-up (GFU) program of IceCube (Aartsen et al. 2018b, 2017c). The combined data set consists of about 1.4 million track-like events. It is dominated by atmospheric neutrinos in the Northern hemisphere and

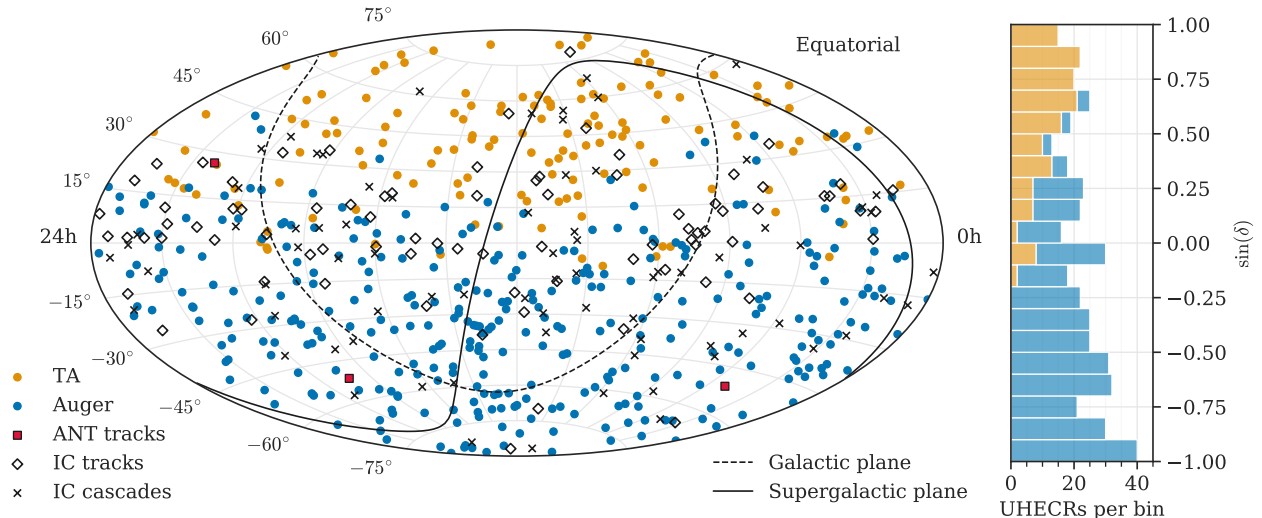


Figure 1. Left: Skymap of the arrival directions of UHECR events and high-energy neutrinos. The high-energy neutrino track-like events from IceCube consists of the HESE, HENU and EHE data sets, while the cascade-like events are only of the IceCube-HESE data sets. From ANTARES, only high-energy tracks are selected for the analyses. Right: A histogram of the declination of UHECR events, separated into Auger and TA contribution.

by atmospheric muons in the Southern hemisphere. The median of the angular resolution (Ψ) is better than 0.5° above energies of a few TeV. Figure 2 shows the median of the angular resolution for the different detector configurations of IceCube, and for data from the ANTARES detector (see subsection 2.2). Note that analysis 1 is not based on the median of the angular resolution, but on the estimator for the angular resolution on an event-by-event basis (σ).

The HESE data set contains 76 cascade-like events and 26 track-like events that have been collected between 2010 and 2017, as presented in Wandkowsky (2018). It consists of neutrinos of all flavors that interacted inside the detection volume, called starting events, with deposited energies ranging between about 20 TeV and 2 PeV. Integrated above 60 TeV, which corresponds to 60 events in total, the percentage of events of astrophysical origin, i.e. the astrophysical purity, is larger than 75 % (Wandkowsky 2018), while the percentage is lower below 60 TeV. The angular resolution is about 1° for track-like events and 15° for cascade-like events above 100 TeV. The resolution of the deposited energy for tracks and cascades is around 10 % (Aartsen et al. 2014a) without accounting for systematic uncertainties, but the cascades have a better correlation with the primary neutrino energy since they deposit most of their energy inside the detector, while tracks do not.

The HENU data set consists of the 35 highest energy track-like events with a reconstructed declination $\geq -5^\circ$, which have been collected between 2009 and 2016 (Haack & Wiebusch 2017) for the measurement of the diffuse muon-neutrino flux (Aartsen et al. 2016). From the original data set starting at ~ 100 GeV, only events of high probability of non-atmospheric origin have been selected by applying an energy threshold of ≥ 200 TeV on the reconstructed muon energy. This corresponds to an astrophysical purity of more than 50 %. The astrophysical purity here is defined as the flux ratio of the astrophysical to the sum of atmospheric and astrophysical differential fluxes and thus depends on the assumed astrophysical flux. For the estimation of the astrophysical purity, the best fit astro-

physical flux from [Aartsen et al. \(2016\)](#) $d\phi/dE = 1.01 \times 10^{-18} \text{ GeV}^{-1} \text{ cm}^{-2} \text{ s}^{-1} \text{ sr}^{-1} (E/100 \text{ TeV})^{-2.19}$ is used as well as the best fit atmospheric flux from the same reference.

The EHE data set consists of 20 events that have been collected between 2008 and 2017 ([Aartsen et al. 2018c, 2017c](#)). The selection is targeting high-energy track-like events of good angular resolution $\leq 1^\circ$. The selection has been optimized to be sensitive for events in the energy range of 0.5 PeV to 10.0 PeV. The integrated astrophysical purity depends on the assumption on the spectrum of astrophysical events at the highest energies, but can be estimated as approximately 60 % purity (see Table 2 in [Aartsen et al. \(2017c\)](#)).

2.2. The ANTARES Neutrino Telescope

The ANTARES telescope ([Ageron et al. 2011](#)) is a deep-sea Cherenkov neutrino detector located 40 km offshore from Toulon, France, in the Mediterranean Sea. The detector is composed of 12 vertical strings anchored at the sea floor at a depth of 2475 m. The strings are spaced at distances of about 70 m from each other, instrumenting a total volume of $\sim 0.01 \text{ km}^3$. Each string is equipped with 25 storeys of 3 optical modules ([ANTARES Collaboration et al. 2002](#)), vertically spaced by 14.5 m, for a total of 885 optical modules. Each optical module houses a 10-inch photomultiplier tube facing 45° downward to optimize the detection of light from upward going charged particles. The detector was completed in 2008.

The ANTARES and IceCube detection principles are very similar (see [subsection 2.1](#)). Particles above the Cherenkov threshold induce coherent radiation emitted in a cone with a characteristic angle of 42° in water. The position, time, and collected charge of the signals induced in the photomultiplier tubes by detected photons are used to reconstruct the direction and energy of events induced by neutrino interactions and atmospheric muons. Trigger conditions based on combinations of local coincidences are applied to identify signals due to physics events over the environmental light background due to ^{40}K decays and bioluminescence ([Aguilar et al. 2007](#)). ANTARES is thus also capable of detecting neutrino charged- and neutral-current interactions of all flavors.

For analysis 1, we use all track-like events from the 11-year data set used for point-source searches (PS) recorded between 2007 and 2017 ([Albert et al. 2018; Illuminati et al. 2019](#)). The high-energy events (HENU) for analyses 2 and 3 are selected from an earlier data set of track-like and cascade-like events collected between 2007 and 2015 ([Albert et al. 2017](#)). In order to ensure a high probability of astrophysical origin for analyses 2 and 3, we require an astrophysical purity $\geq 40\%$ based on the same definition as used for the HENU data set of IceCube. This selection results in a total of three track-like events and no cascade-like events, of which the arrival directions are shown in [Figure 1](#). An overview of the nomenclature is presented in [Table 1](#). The track-like events are combined with the respective IceCube data sets. All events have a good angular resolution that is below 0.4° above 10 TeV ([Albert et al. 2017](#)). Overall, the angular resolution of ANTARES tracks is better than for IceCube tracks for energies below 100 TeV, and comparable around 100 TeV and above. The median angular resolution, Ψ , of the 11-year data set compared to the IceCube PS data set is shown in [Figure 2](#).

Despite the smaller detection volume, the inclusion of ANTARES data significantly improves the all-sky coverage of the neutrino data set used in analysis 1. This is shown in [subsection 4.1](#) and [Figure 5](#) through the relative contribution to the expected number of signal events for the individual PS data sets of ANTARES and IceCube. Particularly in the Southern hemisphere, where the background from

atmospheric muons results in a higher energy threshold in IceCube, the ANTARES data contributes substantially to the signal acceptance for soft source spectra.

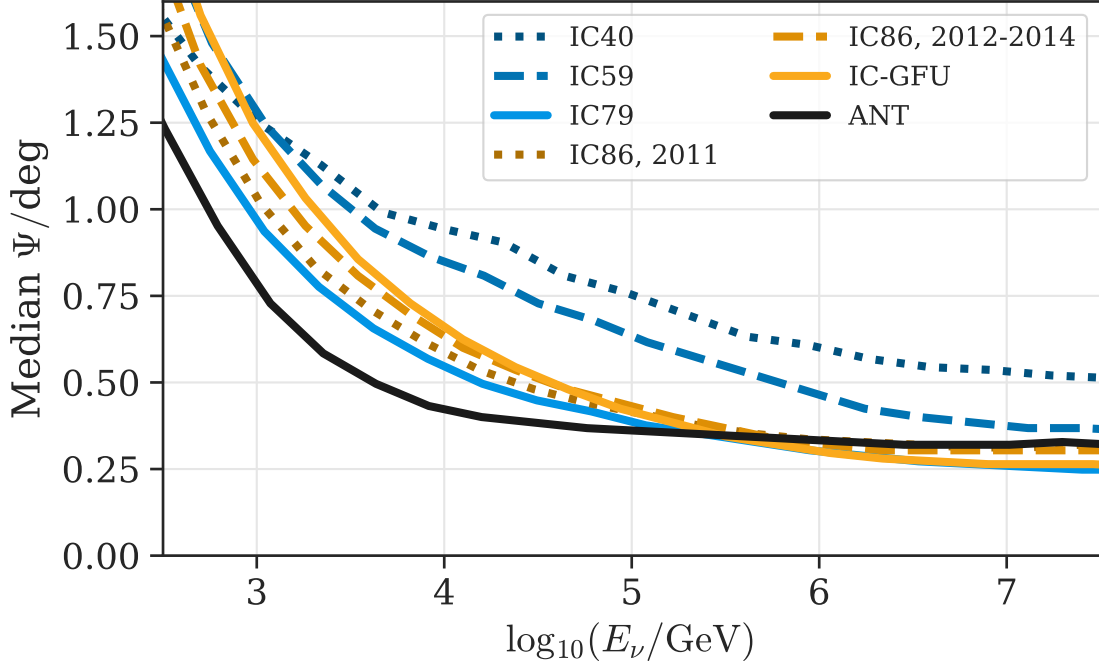


Figure 2. Median of the angular resolution, Ψ , which is the angle between the true neutrino direction and reconstructed muon direction for IceCube and ANTARES point-source data as a function of the true neutrino energy. This is calculated based on simulation data sets. The data from partial detector configurations of IceCube are denoted by the number of operating strings, (IC40, IC59, IC79; [Aartsen et al. 2014c](#)) and are shown in blue. The data of the full detector configuration with 86 strings including the GFU data set ([Aartsen et al. 2017c,d, 2018b](#)) are identified by the years of data taking and are shown in orange. The angular resolution of ANTARES data for the 11-year data set ([Albert et al. 2018; Illuminati et al. 2019](#)) is shown in black.

Detector	Analysis 1	Analysis 2	Analysis 3
ANTARES	PS	HENU	HENU
IceCube	PS	HESE + HENU + EHE	HESE + HENU + EHE

Data set	Description	Topology
PS	Optimized for point-source searches, ν_μ candidates.	Tracks
HESE	High-energy starting events, all flavors.	Tracks and cascades
HENU	High-energy selection of ν_μ candidates.	Tracks
EHE	Extremely-high energy ν_μ candidates.	Tracks

Table 1. Overview over different neutrino data sets used in the different analyses.

2.3. *The Pierre Auger Observatory*

The Pierre Auger Observatory is located in Argentina (32°S, 69°W) at a mean altitude of 1.4 km above sea level (The Pierre Auger Collaboration 2015). The observatory has a hybrid design combining an array of particle detectors at ground (surface detector, SD) and an atmospheric fluorescence detector (FD) for detecting the air showers caused by UHECRs interacting with the atmosphere. The SD array is composed of 1660 water-Cherenkov detectors spread over an area of 3000 km². The SD area is overlooked by the FD, which consists of 27 wide-angle optical telescopes located at four sites. The reconstruction of SD events is described in detail in Aab et al. (2020). The energy estimate is based on the signal at 1000 m from the reconstructed intersection of the shower axis with the ground, which is extracted with a fit of the lateral distribution of signals in the individual detectors. This value is then corrected to take into account the different absorption suffered by showers coming at different angles. Due to the hybrid design of the observatory, this energy estimator is calibrated via the correlation with the near-calorimetric energy measured by the FD with the events observed by both SD and FD. Through this calibration, the energy estimate for SD is done without relying on Monte Carlo. At the energies considered in this work, the systematic uncertainty on the energy scale is 14% (Dawson 2019), the statistical uncertainty on the energy due to the number of triggered SD stations and uncertainties of their response is smaller than 12% (Abreu et al. 2011; Aab et al. 2020), and the angular uncertainty is less than 0.9° (Bonifazi & The Pierre Auger Collaboration 2009).

The UHECR data set used here consists of 324 events observed with the SD between January 2004 and April 2017 (Aab et al. 2018) with reconstructed energies ≥ 52 EeV and zenith angles $\leq 80^\circ$. The data statistics is enlarged with respect to the previously used data set (Aab et al. 2015) by 93 events and includes an updated energy calibration based on a larger number of hybrid events and an improved absorption correction. The angular acceptance translates into a field of view ranging from -90° to 45° in declination. All energies are scaled up by 14% to match both Auger and TA energies on a common energy scale (see subsection 2.4), following the recommendation of the Auger-TA joint working group (Biteau et al. 2019). The celestial distribution of the UHECR arrival directions is shown in Figure 1. The directional exposure as function of declination can be found in Figure 3, which amounts to an integrated geometric exposure of 91 300 km² yr sr.

2.4. *The Telescope Array*

The Telescope Array (TA) is located in Millard County, Utah, USA (39.3°N, 112.9°W) at an altitude of about 1.4 km (Kawai et al. 2008). It consists of a surface detector (SD) array, composed of 507 plastic scintillation detectors of 3 m² each. The SD stations are located on a square grid with 1.2 km separation, which extends over an area of 700 km² (Abu-Zayyad et al. 2012). The TA SD array observes UHECRs with a duty cycle near 100%. With its wide field of view, the SD array covers a range from -15° to 90° in declination. In addition to the SD, there are three fluorescence telescope stations, instrumented with 12 to 14 telescopes each (Tokuno et al. 2012). The telescope stations observe the sky above the SD array and measure the longitudinal development of the air showers as they traverse the atmosphere.

The data set for this analysis follows the selection in Abbasi et al. (2014), which has been updated to 9 years of data in Abbasi et al. (2018). The data set is identical to the data set used for anisotropy analyses presented in Troitsky et al. (2017). It consists of 143 events observed with the SD between May 2008 and May 2017 with reconstructed energies ≥ 57 EeV and zenith angles $\leq 55^\circ$. At these

energies, the angular uncertainty is about 1.5° . The statistical uncertainty on the reconstructed energy is about 15% to 20%, with an additional systematic uncertainty on the energy scale of 21% (Abbasi et al. 2018). All energies are scaled down by -14% to match both Auger and TA energies on a common energy scale (see subsection 2.3), following the recommendation of the Auger–TA joint working group (Biteau et al. 2019).

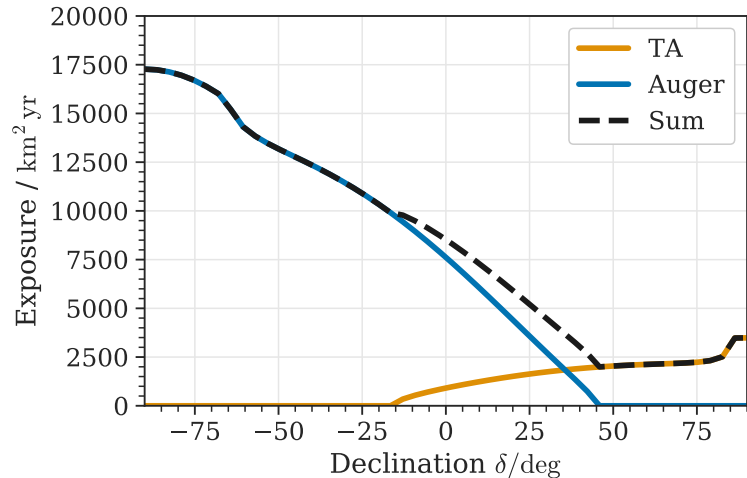


Figure 3. Directional exposures of TA, Auger, and their sum. The underlying geometric exposure functions are derived from Sommers (2001). See also Fig. 1 of Biteau et al. (2019).

The celestial distribution of selected events is shown in Figure 1. The right-hand side of the figure is a histogram of the sine of declination of all UHECR events, showing that TA data substantially contributes to the full-sky exposure of the combined UHECR data set. Figure 3 shows the directional exposure as a function of declination, with an integrated total exposure of $11\,600\text{ km}^2\text{ yr sr}$ (Biteau et al. 2019).

3. MAGNETIC DEFLECTIONS

Despite their extremely high rigidity, UHECRs are deflected in galactic and in extragalactic magnetic fields (GMF/EGMF) by a non-negligible amount. Neither the strength and correlation length of the extragalactic magnetic fields (Durrer & Neronov 2013; Kronberg 1994) nor the distance of the UHECR sources are known well. Measurements of the Faraday rotation of extragalactic sources indicate that the extragalactic magnetic fields are weaker than 1 nG (Pshirkov et al. 2016). Assuming a correlation length of $\sim 1\text{ Mpc}$, this results in a deflection less than 2° for protons of 100 EeV , even at source distances of 50 Mpc . In line with the previously reported results (The IceCube Collaboration et al. 2016), the deflection outside of our galaxy is assumed to be generally weaker than within our galaxy, and it is not modeled explicitly but benchmarked within the uncertainty of the deflection by GMF and the uncertainty of the rigidity due to the unknown composition.

The measurement and modeling of the GMF is a complex task and subject of on-going discussion¹. Among different proposed models, we use the JF2012 (Jansson & Farrar 2012) model and the PT2011

¹ See <https://icrc2021-venue.desy.de> for a recent review by Tess Jaffe on the GMF at ICRC2021: "Constraining Magnetic Fields at Galactic Scales".

(Pshirkov et al. 2011) model to estimate the deflection of the UHECRs in the GMF. Both models consist of a disc and a halo component, while the JF2012 model has an additional x-shaped field component perpendicular to the disc. A propagation simulation has been conducted with a Monte-Carlo approach to estimate the deflection of protons with an energy of 100 EeV that are distributed isotropically outside of the GMF. The resulting deflections are shown in Figure 4, split into the Galactic Northern and Southern hemisphere based on the arrival direction of the proton. The estimated deflection shows a complex structure which differs considerably for the two models. However, the mean deflection is about 3° in both cases. Due to the heavy tails of the distributions, the mean is consistently larger than the median, thus we choose the mean as a conservative deflection estimate. The split into the two hemispheres shows a considerably smaller deflection in the Galactic North than in the Galactic South due to North-South asymmetries present in both models of the GMF. For this work we have chosen a robust benchmark modeling of the effect of the GMF, thus avoiding biases of detailed model uncertainties. The deflection process is assumed to be random, resulting in a symmetric 2D Gaussian distribution of UHECR arrival directions around a given source direction. In reverse, the source position is assumed to be located within the 2D Gaussian distribution around the arrival direction of a UHECR event. The standard deviation of the Gaussian deflection, σ_{MD} , depends on a scaling factor, C , and inversely on the energy of the UHECR event, E_{CR}

$$\sigma_{\text{MD}} = \frac{D_0 \cdot C}{E_{\text{CR}}/100 \text{ EeV}}. \quad (1)$$

The default deflection, D_0 , for $C = 1$ and $E_{\text{CR}} = 100 \text{ EeV}$ is derived from the mean of the deflection values obtained with the simulation, which are shown in Figure 4. Note that the deflection is usually a 2D quantity with (x, y) coordinates, which in Figure 4 is projected to the absolute value, i.e. $\sqrt{x^2 + y^2}$. Furthermore, larger and thus more conservative values of the deflection will be tested to include an uncertainty of the GMF model. The scaling factor C thus accounts for uncertainties of both GMF model and UHECR charge, which is not known on an event-by-event basis at highest energies.

Analysis 1 uses a default deflection of $D_0 = 3^\circ$ over the whole sky, while analysis 2 uses $D_{\text{North/South}} = (2.4^\circ, 3.7^\circ)$ for UHECRs with arrival directions from the Galactic Northern and Southern hemisphere, respectively. The different choices have been made based on the respectively better sensitivity for the two analyses. Analysis 1 and 2 implement the deflection into their methods as described in the respective sections 4.1 and 4.2. Analysis 3 employs a model-independent approach with respect to the UHECR deflection.

4. ANALYSIS METHODS

4.1. Unbinned neutrino point-source search with UHECR information

The goal of analysis 1 is to find point-like neutrino sources that are spatially correlated with UHECR arrival directions within a region derived from their magnetic deflection estimate. The search for neutrino sources utilizes the unbinned maximum-likelihood analysis commonly used in IceCube (Aartsen et al. 2017d, 2019, 2020b). This enables an easy combination of the high-statistics, full-sky neutrino data sets, which are the PS data sets of IceCube and ANTARES described in subsection 2.1 and subsection 2.2, respectively. In addition to this standard method, the magnetic deflection regions, defined by the UHECR arrival directions, energy, and scaling factor, are used for constraining the possible source regions.

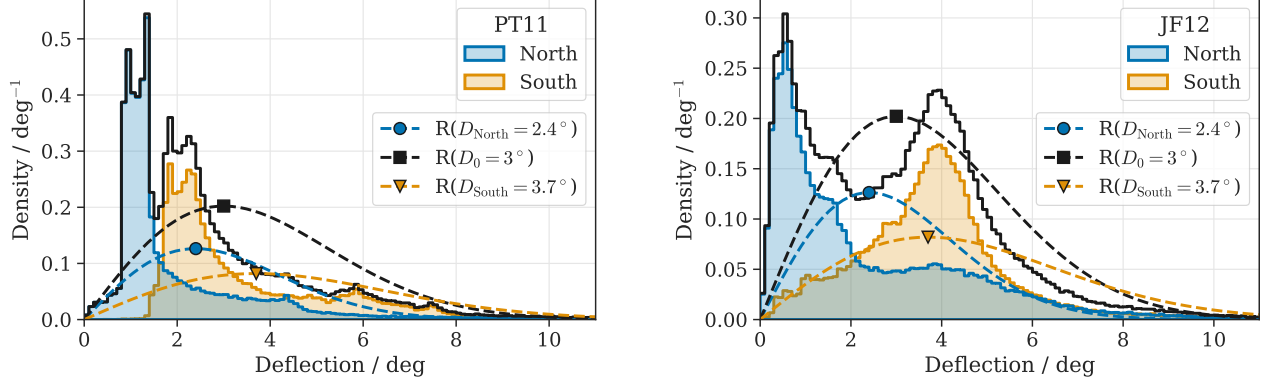


Figure 4. Deflection simulation for protons of 100 EeV and two different galactic magnetic models: PT2011 (Pshirkov et al. 2011) and JF2012 (Jansson & Farrar 2012). Shaded areas in blue and orange show the histogram split into Galactic Northern and Southern hemispheres, with their sum shown as black line. Additionally, Rayleigh PDFs are shown in the same colors; a Rayleigh function with mode σ is the 1D projection of a symmetric 2D-Gaussian function with width σ , with the projection being $(x, y) \rightarrow \sqrt{x^2 + y^2}$. The position of the markers indicate the mode of the Rayleigh PDF and thus the value of the default deflection, D . Note that the integrals of the split PDFs are normalized to 0.5, while the integrals of the full PDFs are normalized to 1.

The unbinned neutrino likelihood in the source direction $\vec{\Omega} = (\alpha, \delta)$ in right ascension and declination consists of the sum of a signal PDF, S , and a background PDF, B

$$\mathcal{L}(n_s, \gamma) = \prod_{j=1}^7 \prod_{i=1}^{N_j} f_j(\sin \delta, \gamma) \frac{n_s}{N_j} \cdot S(\vec{\Omega}_i, E_i, \sigma_i | \gamma, \vec{\Omega}) + \left(1 - f_j(\sin \delta, \gamma) \frac{n_s}{N_j}\right) \cdot B(\delta_i, E_i). \quad (2)$$

The likelihood product with index i runs over all neutrino events within each data set with index j (see subsection 2.1 and subsection 2.2). The likelihood product with index j runs over all data sets to yield the final likelihood function. The likelihood combination of the seven data sets by ANTARES and IceCube is thus handled the same as described in Aartsen et al. (2017d). The signal and background PDFs, S and B , are evaluated for four observables per neutrino event, weighted with the number of signal events over total number of events per data set, n_s/N_j . The observables are the reconstructed right ascension and declination, summarized as $\vec{\Omega}_i = (\alpha_i, \delta_i)$, reconstructed energy, E_i , and angular error estimator, σ_i . The signal PDF consists of two terms: the first term is a declination-dependent reconstructed energy distribution, where the underlying neutrino flux is modeled as a power law

$$\frac{d\Phi^\nu}{dE} = \frac{dN^\nu}{dE dA dt d\Omega} = \Phi_0^\nu \cdot \left(\frac{E}{1 \text{ GeV}}\right)^{-\gamma}. \quad (3)$$

Here, Φ_0^ν is the flux normalization, 1 GeV is the corresponding pivot energy, and γ is the spectral index of the power law. The second term of the signal PDF is a spatial term modeled as a Gaussian with the width, σ_i , given by the angular error estimator of each neutrino candidate on an event-by-event basis. The background PDF is determined as function of reconstructed energy, E_i , and declination, δ_i , from randomized experimental data. A full description of the signal and background PDFs, S and B , can be found in Aartsen et al. (2017d). The proportionality factor, $f_j(\sin \delta, \gamma)$, is

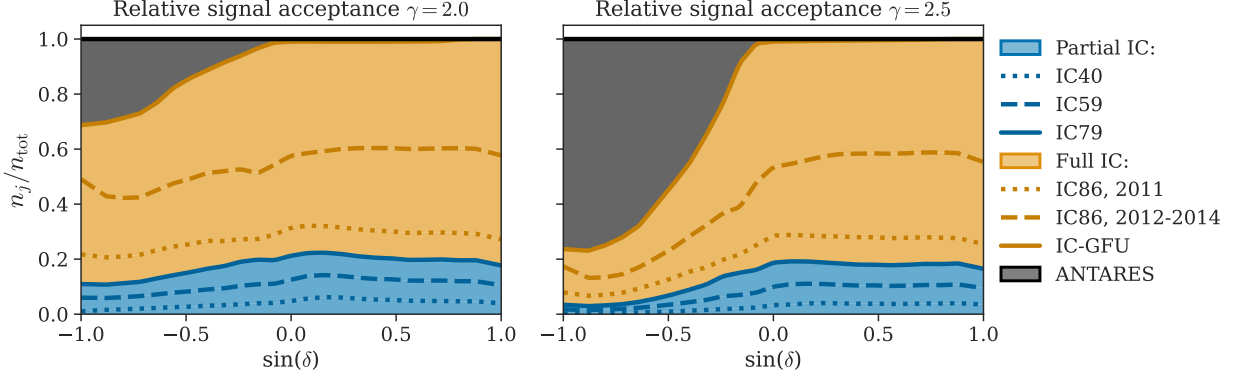


Figure 5. The relative signal contribution, n_j/n_{tot} , for analysis 1 of the different configurations of IceCube and the ANTARES point-source data set as a function of the declination δ . The left plot shows a hard underlying power-law signal spectrum (Equation 3) with index $\gamma = 2.0$, while the right plot shows a softer spectrum with $\gamma = 2.5$. The relative signal contributions from partial detector configurations of IceCube are shown in blue, while the contributions of the full detector configuration of IceCube with 86 strings are shown in orange. The ANTARES contribution is shown in gray. The lines as listed in the rightmost legend indicate the contributions from each data set individually.

the relative signal acceptance per neutrino data set calculated from the expected number of signal events via

$$f_j(\sin \delta, \gamma) = \frac{n_j}{n_{\text{tot}}} = \frac{T^j \int (d\Phi^\nu/dE) A_{\text{eff}}^j(E, \sin \delta) dE}{\sum_{j=1}^7 T^j \int (d\Phi^\nu/dE) A_{\text{eff}}^j(E, \sin \delta) dE}. \quad (4)$$

This factor is used to correctly weight the signal contribution of each data set j for a given source declination and spectral index. Per data set j , the livetime is denoted with T^j and the effective area is denoted with A_{eff}^j . Figure 5 shows the proportionality factor of each data set as a function of declination for two spectral indices, $\gamma = 2.0$ and 2.5 . Note that all data sets are evaluated with the same formulation of the likelihood function as used by IceCube, instead of combining different formulations as described in Albert et al. (2020).

The best-fit signal parameters, \hat{n}_s and $\hat{\gamma}$, at a given source position, $\vec{\Omega}$, are obtained with the maximum-likelihood method. The number of events and the proportionality factor are related to the neutrino flux using the respective livetime and effective area of each data set via

$$n_s = \sum_{j=1}^7 T^j \int \frac{d\Phi^\nu}{dE} A_{\text{eff}}^j(E, \sin \delta) dE. \quad (5)$$

The corresponding significance of a source at position $\vec{\Omega}$ is evaluated using a likelihood ratio test, which yields the test statistic (TS)

$$\text{TS}_\nu(\vec{\Omega}) = 2 \log \left(\frac{\mathcal{L}(\hat{n}_s, \hat{\gamma})}{\mathcal{L}(n_s = 0)} \right) \Big|_{\vec{\Omega}}. \quad (6)$$

Here, the null hypothesis is defined via $n_s = 0$, representing the case of no neutrino sources in the vicinity of UHECR events. Instead of searching for a single neutrino source, the whole sky is searched

on a HEALpix (Górski et al. 2005) grid with a resolution of approximately 0.2° . This results in a skymap of the TS values at each grid center, $\vec{\Omega}_{\text{grid}}$.

The second step is to combine the neutrino likelihood with the information provided by UHECR events and their deflection estimate. The deflection estimate for one UHECR with index k and arrival direction $\vec{\Omega}_k^{\text{CR}}$, which possibly originated in the direction of $\vec{\Omega}_{\text{grid}}$, is defined as a 2D Gaussian. Its width is the quadratic sum of the magnetic deflection estimate, σ_{MD} of Equation 1, and the UHECR angular reconstruction error, σ_{CR}^2 , which is 0.9° for Auger events and 1.5° for TA events

$$\mathcal{P}_k \propto \exp\left(-\frac{(\vec{\Omega}_{\text{grid}} - \vec{\Omega}_k^{\text{CR}})^2}{2(\sigma_{\text{MD}}^2 + \sigma_{\text{CR}}^2)}\right). \quad (7)$$

The term \mathcal{P}_k acts as a spatial constraint, which is multiplied to the neutrino likelihood function defined in Equation 2 via $\mathcal{L} \rightarrow \mathcal{L} \cdot \mathcal{P}_k$. Effectively, the constraint is added as a logarithmic term to the neutrino TS defined for each grid point in Equation 6 via $\text{TS} \rightarrow \text{TS} + 2 \cdot \log(\mathcal{P}_k)$. Finally, the maximum of the combined UHECR-neutrino TS is found at the best-fit grid point, $\hat{\vec{\Omega}}_{\text{grid}}$, via

$$\text{TS}_k^{\text{comb}}(\hat{\vec{\Omega}}_{\text{grid}}) = \max\left(\text{TS}_\nu(\vec{\Omega}_{\text{grid}}) - \frac{(\vec{\Omega}_{\text{grid}} - \vec{\Omega}_k^{\text{CR}})^2}{\sigma_{\text{MD}}^2 + \sigma_{\text{CR}}^2}\right) \quad (8)$$

The maximum marks the neutrino-source candidate which is the most-likely counterpart to the respective UHECR event used to calculate the spatial constraint. The normalization in Equation 7 adds only a constant term to the TS, which can be omitted when calculating significances and p -values based on pseudo-experiments (see below). As a third, final step, this procedure is repeated for all UHECRs and all obtained TS values are added up yielding the final test statistic. This search strategy was first developed in the context of this point-source correlation analysis and first outlined in sec. 4 of Schumacher (2019). It has already been applied also to other neutrino correlation searches with spatially extended source localization, namely the correlation with ANITA events (Aartsen et al. 2020c) and with gravitational wave events (Aartsen et al. 2020d). Note that the analysis described here is improved with respect to the previous search (The IceCube Collaboration et al. 2016, sec. 5), as it models the displacement of a point-like neutrino source with respect to the UHECR arrival direction based on the assumed magnetic deflection. Here, the position and flux of a point-like source are fit in the vicinity of the UHECR direction, while in the previous search, a spatially-extended neutrino emission around the UHECR direction was fit.

Six different signal hypotheses are tested, which are characterized by a lower cut on the UHECR energy, $E_{\text{CR}} > E_{\text{cut}}$ with $E_{\text{cut}} \in \{70, 85, 100\}$ EeV, and the scaling factor of the deflection estimate, $C \in \{1, 2\}$. The lower energy cut is a threshold for selecting only the highest-energy UHECRs with the lowest deflection for this analysis. No analogous energy cut is applied to the neutrino data. The scaling factor C is a model parameter for scaling the baseline magnetic deflection, and it is not derived from the UHECR data. The baseline magnetic deflection is $D_0 = 3^\circ$ for all UHECRs, which is then converted into the spatial constraint of an individual UHECR event using Equation 1 and Equation 7. The corresponding sensitivity and 3σ -discovery potential are evaluated based on the normalization of the neutrino flux per source, Φ_0' (see Equation 3). The 3σ threshold is chosen, since the background expectation needs to be calculated based on pseudo-experiments, as described in the next paragraph. A 5σ -discovery potential is computationally too expensive to be calculated for the

various hypotheses. Sensitivity is defined as the expected median upper limit at 90% confidence level on Φ_0' in case of a null measurement, while the discovery potential is defined as the median of Φ_0' required for a rejection of the background hypothesis with 3σ significance.

Both sensitivity and discovery potential are calculated based on data challenges, for which signal-like and background-like pseudo-experiments (PEs) are generated. Since the calculation is based on PEs, the constant term in Equation 7 and Equation 8, i.e. the normalization of the constraint term, can be omitted. For all signal and background PEs, the UHECR arrival directions are kept fixed. The background PEs are obtained by randomizing the experimental neutrino data in right ascension. The signal PEs reflect the six different signal hypotheses; one signal PE is based on experimental neutrino data randomized in right ascension, to which Monte-Carlo neutrino events, representing a neutrino source, are added. The location of this neutrino source is chosen randomly within the spatial deflection constraint of one UHECR event. This way, we mimic a neutrino source that is displaced with respect to the UHECR direction due to the UHECR deflection. In the baseline model of the signal PEs, all UHECR events have such an artificial neutrino source in their vicinity. For one PE, all neutrino sources have an E^{-2} power-law spectrum and the same flux normalization. Note that the UHECR energy cut and scaling factor used to generate the spatial constraints for the likelihood function are the same as for determining the neutrino source location.

We generate additional signal PEs by varying the fraction of UHECR events, f_{corr} , with a neutrino source in their vicinity. This mimics signal models where not all UHECRs have a corresponding neutrino source in the vicinity of their arrival direction. Thus, the number of neutrino sources is determined by the rounded-up product of the correlation fraction with the numbers of UHECRs, $N_{\nu}^{\text{src}} = \lceil f_{\text{corr}} N_{\text{CR}} \rceil$, where N_{CR} is the number of UHECRs passing the energy cut. We choose the correlation fraction from three discrete values, $f_{\text{corr}} \in \{1, 0.5, 0.1\}$, where $f_{\text{corr}} = 1$ represents the baseline model. Note that the correlation fraction is only used to choose the number of neutrino sources in the signal PEs, while in a real experimental data, it is not known a priori which UHECRs have a correlated neutrino source and which do not. For $f_{\text{corr}} < 1$, only a number of $N_{\nu}^{\text{src}} < N_{\text{CR}}$ of randomly selected UHECRs will have a correlated neutrino source in the signal PEs. Independent of the correlation fraction, the TS values of all UHECR constraints are added up, since in real experimental data it would not be known which UHECRs have a correlated neutrino source. The sensitivity and 3σ -discovery potential in terms of the flux normalization per neutrino source for all signal models and hypotheses are reported in Table 2, which are also shown in Figure 6. We see that a smaller correlation fraction increases the flux normalization per neutrino source for both sensitivity and 3σ -discovery potential. This is expected since a smaller correlation fraction corresponds to fewer neutrino sources, which in turn need to have a higher flux normalization to be detected by the analysis.

It is noticeable that for a small correlation fraction of $f_{\text{corr}} = 0.1$, the signal model with a larger scaling factor of $C = 2$ yields a better 3σ -discovery potential than the smaller scaling factor of $C = 1$. This is unexpected, as a smaller UHECR deflection and thus a smaller spatial constraint should yield more accuracy in detecting the corresponding neutrino sources. However, the amount of sky covered by the constraints does not grow uniformly with the scaling factor and numbers of UHECRs, since the UHECR spatial constraints can overlap. In the case of a small correlation fraction, a high neutrino flux per source is required to reach the 3σ -discovery potential due to the small number of sources

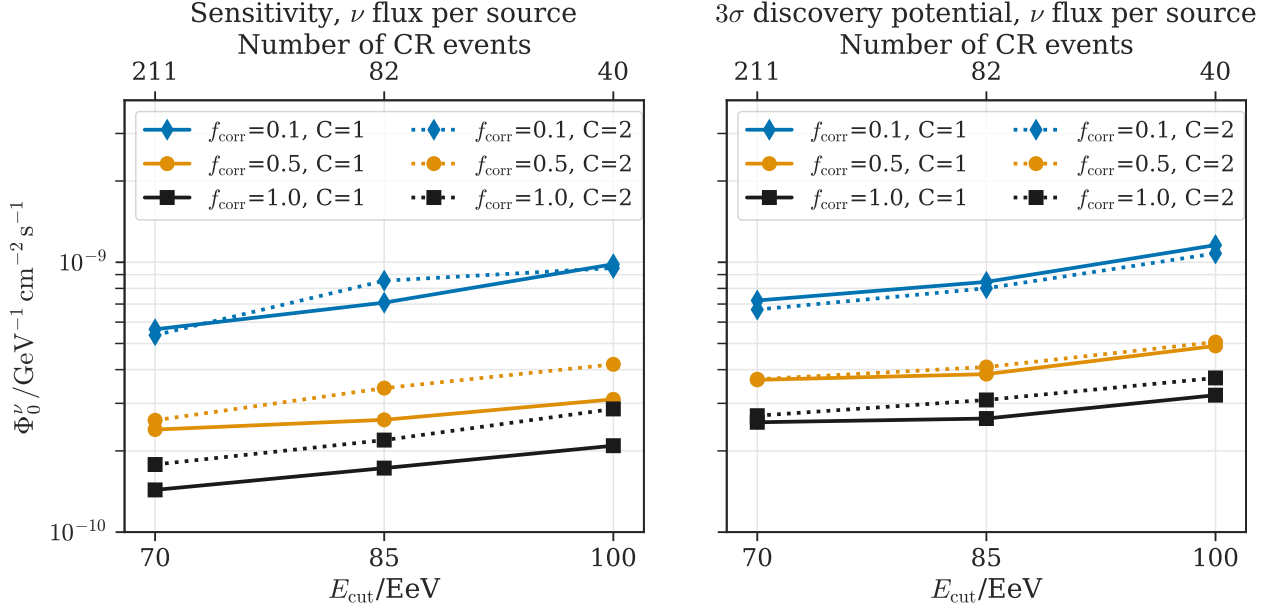


Figure 6. Sensitivity (left) and 3σ -discovery potential (right) of the neutrino flux per source as function of the UHECR energy cut in EeV, for the three correlation fractions and for the two scaling factors we used.

present². A closer study showed that in the case of few, but strong neutrino sources, it is beneficial to search a larger area of the sky for sources so that fewer of them are missed. This effect is thus caused by an interplay between deflection size, number of UHECRs and relatively high neutrino flux per source in this particular case.

4.2. Unbinned likelihood-stacking analysis of UHECRs and high-energy neutrinos

The second analysis is based on using the neutrinos with a high probability of astrophysical origin as markers for the location of the sources of UHECRs and neutrinos. The UHECR events are stacked using an unbinned likelihood analysis with the arrival directions of the high-energy neutrinos as the source positions. The signal hypothesis is defined by the number of UHECR events, which are clustered around the neutrino arrival directions, as well as the size of the magnetic deflection. The background hypothesis is defined by an isotropic flux of UHECRs. This approach is thus complementary to the point-source correlation analysis, where the UHECR events are used as source markers and an isotropic flux of neutrinos defines the background hypothesis. The logarithm of the likelihood function is defined as

$$\log \mathcal{L}(n_s) = \sum_{i=1}^{N_{\text{Auger}}} \log \left(\frac{n_s}{N_{\text{CR}}} S_{\text{Auger}}^i + \frac{N_{\text{CR}} - n_s}{N_{\text{CR}}} B_{\text{Auger}}^i \right) + \sum_{i=1}^{N_{\text{TA}}} \log \left(\frac{n_s}{N_{\text{CR}}} S_{\text{TA}}^i + \frac{N_{\text{CR}} - n_s}{N_{\text{CR}}} B_{\text{TA}}^i \right), \quad (9)$$

where the free parameter is the total number of UHECR signal events, n_s . The sums run over all UHECR events in the respective data set, i.e. N_{Auger} and N_{TA} , where the total number of UHECR events is $N_{\text{CR}} = N_{\text{Auger}} + N_{\text{TA}}$. In contrast to the likelihood function of analysis 1, the signal PDFs, S_{Auger}^i and S_{TA}^i , and the background PDFs, B_{Auger}^i and B_{TA}^i , are stacked for all high-energy neutrinos

² There are 22, 9 and 4 sources for $f_{\text{corr}} = 0.1$ and the energy cuts of $E_{\text{cut}} \in \{70, 85, 100\}$ EeV, respectively.

such that n_s is a global parameter. The background PDFs per UHECR detector, B_{det}^i , are the normalized expectations for an isotropic UHECR flux as function of declination, which correspond to the normalized detector exposures (see [Figure 3](#)). The signal PDF per UHECR detector is defined as

$$S_{\text{det}}^i(\vec{\Omega}_i, E_i) = R_{\text{det}}(\delta_i) \cdot \sum_{j=1}^{N_\nu} S_j(\vec{\Omega}_i, \sigma(E_i)) \quad \text{with } \sigma^2 = \sigma_{\text{MD}}^2 + \sigma_{\text{CR}}^2, \quad (10)$$

as a function of the UHECR arrival direction, $\vec{\Omega}_i$, and energy, E_i . The term R_{det} is the relative exposure of each detector as a function of the declination per UHECR event, δ_i . [Figure 3](#) shows the absolute directional exposures, which are each normalized to 1 over the whole sky to obtain R_{det} . The sum runs over all neutrino events, N_ν , where the terms of $S_j(\vec{\Omega}_i, \sigma(E_i))$ are the spatial likelihood maps obtained from the neutrino directional reconstruction smeared with the UHECR uncertainty with width $\sigma(E_i)$ (see [Equation 7](#)). Thus, these terms are PDFs representing the total uncertainty on the common source position of UHECR event i and neutrino event j , evaluated at the UHECR arrival direction, $\vec{\Omega}_i$. Similar to analysis 1, three different deflections corresponding to scaling factors of $C \in \{1, 2, 3\}$ are represented in the signal terms of the likelihood function. Again, C is a model parameter that scales the magnitude of the deflection and it is not derived from UHECR data. Depending on whether the UHECR arrival direction is in the Northern or Southern Galactic Hemisphere (see [Figure 4](#)), the baseline magnetic deflection is thus

$$D = C \cdot (D_{\text{North}}, D_{\text{South}}) = C \cdot (2.4^\circ, 3.7^\circ) \quad \text{with } C \in \{1, 2, 3\}, \quad (11)$$

The final value of the deflection, σ_{MD} , is then calculated based on the UHECR energy using [Equation 1](#).

The best-fit of the number of signal events, \hat{n}_s , is found with a maximum likelihood estimation. The resulting test statistic is defined as the likelihood ratio of the maximum likelihood over the background likelihood with $n_s = 0$

$$\text{TS} = 2 \log \frac{\mathcal{L}(\hat{n}_s)}{\mathcal{L}(n_s = 0)}. \quad (12)$$

The significance is then determined based on the assumption that the background expectation is distributed according to a χ^2 function with one degree of freedom, which has been verified using background-like PEs. The test statistic is calculated separately for all track-like and all cascade-like neutrino events, and separately for the three different deflections. The analysis approach is essentially the same as published in [The IceCube Collaboration et al. \(2016\)](#), except for the updated magnetic deflection values, which are split into the Galactic Northern and Southern Hemisphere as described in [section 3](#).

The sensitivity and the 3σ -discovery potential in terms of n_s are obtained with data challenges based on PEs. Here, the neutrino arrival directions are kept fixed per PE, while the UHECR arrival directions and energies are generated resembling the signal and background hypothesis. For the background PEs, all UHECR arrival directions are derived from an isotropic flux and thus according to the exposure of the respective UHECR experiments. The energies of the UHECR events are sampled from a power-law proportional to $E^{-4.2}$ for the Auger events and to $E^{-4.5}$ for the TA events, same as in [The IceCube Collaboration et al. \(2016\)](#). For the signal PEs, a number of n_s

UHECR arrival directions are distributed randomly based on their respective spatial signal terms in Equation 10, $S_j(\vec{\Omega}_i, \sigma(E_i))$. Note that all UHECRs have the same scaling factor, corresponding to the respective signal hypothesis as implemented in the likelihood function. The sensitivity and 3σ -discovery potential for the three different benchmark values of C are presented in Table 3, separately for the track-like and cascade-like neutrino events. We find that the sensitivity and 3σ -discovery potential using neutrino tracks requires much fewer UHECRs than when using neutrino cascades, which is expected due to the large differences in angular reconstruction uncertainty of the two event topologies.

4.3. Two-point angular correlation of UHECRs and high-energy neutrinos

The 2pt-correlation analysis relies on counting pairs of UHECRs and the high-energy neutrinos, where the angular separation between their arrival directions is within a maximum angular separation, α . The observed number of pairs within this radius, $n_{\text{obs}}(\alpha)$, is compared to the mean number of pairs expected from pure background, i.e. uncorrelated arrival directions, $\langle n_{\text{bckg}}(\alpha) \rangle$. The relative excess of pairs is defined as

$$\frac{n_{\text{obs}}(\alpha)}{\langle n_{\text{bckg}}(\alpha) \rangle} - 1. \quad (13)$$

As the separation angle is not known a-priori, angles between 1° and 30° in steps of 1° are tested. The angle with the largest deviation from the background expectation is chosen after the scan.

The significance of the experimental result is calculated with respect to background PEs. Similar to analysis 2, the background PEs are generated with a fixed set of neutrino arrival directions, and uncorrelated UHECR arrival directions are generated according to the exposure of the respective UHECR experiments. The energies are sampled from the same spectra as described in subsection 4.2. As a cross-check, additional background PEs are generated with the fixed set of UHECR arrival directions, and neutrino arrival directions are randomized in right ascension. The different types of background PEs approximate an isotropic flux of UHECR and high-energy neutrinos, respectively.

Note that this analysis does not include an assumption of the magnetic deflection of UHECRs, which makes it a robust and model-independent approach. The analysis approach is the same as published in The IceCube Collaboration et al. (2016).

5. RESULTS

5.1. Unbinned neutrino point-source search with UHECR information

The test statistic of experimental data is obtained with the neutrino point-source correlation analysis as described in subsection 4.1, assuming the six different combinations of signal parameters, i.e. combinations of scaling factor, C , and lower energy cut, E_{cut} . Each of the six experimental TS values is evaluated with respect to the corresponding distribution of TS obtained from background-like PEs. The resulting p -values for all six tests are listed in Table 2. The smallest p -value (9.7%) is found for the scaling factor of $C = 2$ and an UHECR energy cut of $E_{\text{cut}} = 85 \text{ EeV}$. The p -value increases to 24% when correcting for the trials due to the six correlated tests. This correction is based on the combined distribution of all minimum p -values of the background PEs. All p -values are fully compatible with the background hypothesis of no resolved neutrino sources in spatial correlation with the UHECRs considering the assumed signal models. Based on the experimental TS value, 90% C.L. upper limits on the normalization of the flux of neutrino sources correlated with UHECR arrival

directions are reported in the last three rows of Table 2. In the case of the single p -value larger than 50% found for $C = 1$ and $E_{\text{cut}} = 100 \text{ EeV}$, the limits are set equal to the sensitivity in order to not over-estimate the limits based on an under-fluctuation in data. In addition to the baseline correlation fraction of 100%, the limits are calculated for two smaller correlation fractions of 50% and 10%. In these cases, the limits are relaxed by about 40% to 60% for $f_{\text{corr}} = 0.5$ compared to $f_{\text{corr}} = 1$, and by about a factor of 3 to almost 5 for $f_{\text{corr}} = 0.1$ compared to $f_{\text{corr}} = 1$.

Analysis parameters						
$D_0 \cdot C$	3°	3°	3°	6°	6°	6°
E_{cut}	70 EeV	85 EeV	100 EeV	70 EeV	85 EeV	100 EeV
Number of neutrino sources, N_{ν}^{src}						
$f_{\text{corr}} = 0.1$	22	9	4	22	9	4
$f_{\text{corr}} = 0.5$	106	41	20	106	41	20
$f_{\text{corr}} = 1$	211	82	40	211	82	40
Sensitivity						
$f_{\text{corr}}=0.1$	5.6	7.1	9.8	5.4	8.5	9.5
$f_{\text{corr}}=0.5$	2.4	2.6	3.1	2.6	3.4	4.2
$f_{\text{corr}}=1$	1.4	1.7	2.1	1.8	2.2	2.9
3σ disc. potential						
$f_{\text{corr}}=0.1$	7.2	8.5	11.6	6.7	8.0	10.8
$f_{\text{corr}}=0.5$	3.7	3.8	4.9	3.7	4.1	5.1
$f_{\text{corr}}=1$	2.6	2.6	3.2	2.7	3.1	3.7
90% C.L. upper limit						
$f_{\text{corr}}=0.1$	6.4	9.2	9.8	6.7	10.9	10.6
$f_{\text{corr}}=0.5$	2.8	3.6	3.1	3.3	4.7	4.5
$f_{\text{corr}}=1$	1.7	2.3	2.1	2.3	3.2	3.1
Pre-trial p-value						
	0.33	0.23	>0.5	0.19	0.097	0.43

Table 2. Sensitivity, discovery potential and 90% C.L. upper limit for the different analysis parameters, which are the UHECR energy cut, E_{cut} , magnetic deflection, $D_0 \cdot C$, and correlation fraction, f_{corr} , for the point-source correlation analysis. The values are given as normalization of the neutrino flux per source in the unit of $10^{-10} \text{ GeV}^{-1} \text{ cm}^{-2} \text{ s}^{-1}$. The neutrino flux per source is modeled with a power-law of the form $d\Phi/dE = \Phi_0 \cdot (E/1 \text{ GeV})^{-2}$. The last row states all six experimentally obtained pre-trial p -values with respect to the null hypothesis of an isotropic neutrino flux.

5.2. Unbinned likelihood-stacking analysis of UHECRs and high-energy neutrinos

The UHECR stacking analysis is performed for track-like and cascade-like high-energy neutrinos separately for three different scaling factors of $C \in \{1, 2, 3\}$. This results in six p -values with respect to the background hypothesis of an isotropic flux of UHECRs, of which none is significant. The smallest p -value is 0.26, which is found for cascades and the largest scaling factor of $C = 3$, corresponding to the benchmark deflection in the Northern and Southern Galactic hemisphere of $(7.2^\circ, 11.1^\circ)$. Based on the observed TS values, 90% C.L. limits on the number of UHECR events correlated to the high-energy neutrinos are calculated using the PEs of the corresponding signal hypothesis for each of the

Analysis parameters			
$D_{N/S} \cdot C$	(2.4°, 3.7°)	(4.8°, 7.4°)	(7.2°, 11.1°)
Sensitivity			
tracks	9.8	9.8	10.3
cascades	57	61	64
3σ disc. potential			
tracks	20	21	21
cascades	113	129	135
90% C.L. upper limit			
tracks	9.8	9.8	10.3
cascades	55	76	101
Pre-trial p-values			
tracks	>0.5	>0.5	>0.5
cascades	>0.5	0.38	0.26

Table 3. Sensitivity, 3σ discovery potential, and 90% C.L. upper limits in terms of number of UHECRs (n_s , c.f. Equation 9) as well as the pre-trial p -values for the UHECR stacking analysis with the samples of high-energy tracks and cascades assuming an isotropic flux of UHECRs.

six tests. Since all p -values using the track-like neutrinos are larger than 0.5, the limits are set equal to the sensitivity in order to not over-estimate the limits based on an under-fluctuation in data. All p -values and the corresponding limits are reported in Table 3 together with the sensitivity and discovery potential.

5.3. Two-point angular correlation of UHECRs and high-energy neutrinos

The 2pt-correlation analysis is applied to the sets of neutrino tracks and cascades separately, as well as for the background hypothesis of an isotropic UHECRs flux and an isotropic high-energy neutrino flux. The significance of the result with respect to the background hypothesis is corrected for the scan over the separation angles. This results in four p -values and four respective best-fit angular separation, as listed in Table 4. The largest deviation from an isotropic flux of high-energy neutrinos (p -value=15%) is found using cascades and a maximum angular separation of 16°. None of the p -values show a significant result, thus the results are all compatible with their respective background hypothesis. The relative excesses of pairs with respect to an isotropic distribution of neutrinos as a function of the separation angle are shown in Figure 7, separately for neutrino tracks and cascades.

6. CONCLUSIONS

Three complementary analyses have been performed on the UHECR data sets provided by the Pierre Auger and the Telescope Array Collaborations combined with the high-energy and full-sky neutrino data sets provided by the IceCube and ANTARES Collaborations. For both the UHECR and neutrino data sets, the combination of data from the two respective observatories provides a field of view over the entire sky. None of the analyses found a result incompatible with the assumed background hypotheses of either an isotropic neutrino flux or an isotropic UHECR flux. This is an

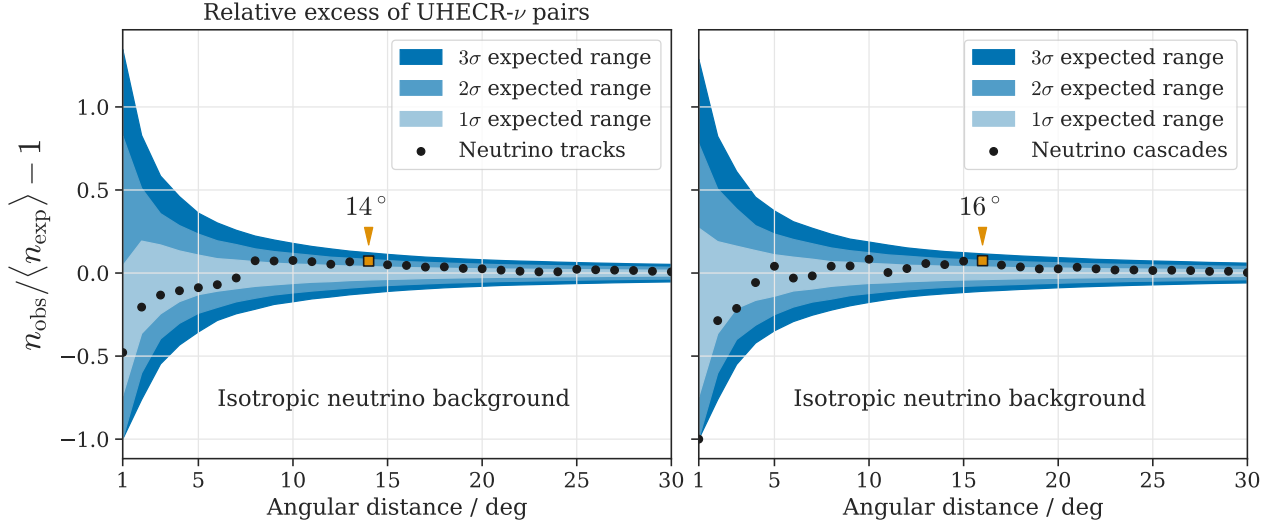


Figure 7. Relative excess of pairs, $n_{\text{obs}}/\langle n_{\text{exp}} \rangle - 1$, as a function of the maximum angular separation of the neutrino and UHECR pairs. The experimental result is shown as black dots, while the blue color bands show the regions containing the 1, 2 and 3σ fluctuations from background PEs based on an isotropic distribution of high-energy neutrinos. The results for the track-like neutrinos are shown on the left, and for the cascade-like neutrino on the right.

Event type	background hypothesis	separation	post-trial p -value
tracks	isotropic neutrinos	14°	0.23
cascades	isotropic neutrinos	16°	0.15
tracks	isotropic UHECRs	10°	>0.5
cascades	isotropic UHECRs	16°	0.18

Table 4. Post-trial p -value and best-fit angular separation for the 2pt-correlation analysis obtained with the neutrino data sets of high-energy tracks and cascades, as stated in the first column. The p -values are corrected for choosing the largest deviation out of all maximum angular separations. The respective background hypotheses are stated in the second column.

important update on the results reported in [The IceCube Collaboration et al. \(2016\)](#), where p -values close to the 3σ level were reported when applying analyses 2 and 3 to cascade-like neutrino events.

Based on the results, 90% C.L. upper limits are calculated for analysis 1 on the flux of neutrinos from point-like sources correlated with UHECRs, and for analysis 2 on the number of UHECR events correlated with high-energy neutrinos. Analysis 1 reports upper limits on the correlated neutrino flux per source given different sets of parameters that make assumptions about the lower cut on the UHECR energy and the fraction of UHECRs with a correlated neutrino source, as well as about a scaling factor of the magnetic deflection (see [Table 2](#)). Analysis 2 reports upper limits on the number of correlated UHECR events with either track-like or cascade-like neutrinos depending on the scaling factor of the magnetic deflection (see [Table 3](#)). This is the first time that upper limits from a direct correlation search of UHECRs and neutrinos are reported.

These limits are calculated based on the assumed signal and background hypotheses and are thus based on the parameters of the respective signal models. In the following, we discuss the limitations of these signal models in the light of underlying assumptions made for the neutrino-UHECR correlation. There are several plausible explanations why we have not observed a significant correlation of UHECRs and neutrinos.

Neutrino sources are presumably distributed over the whole universe, and the emitted neutrinos are able to reach Earth without deflection or absorption. For example, the first neutrino source identified with compelling evidence, TXS 0506+056 (Aartsen et al. 2018a,b), is located at a redshift of $z = 0.34$ (Paiano et al. 2018), corresponding to a comoving distance of about 1.3 Gpc. This is beyond the assumed horizon for UHECRs sources in the local universe of up to about 200 Mpc. Therefore, the fraction of correlated sources in the local universe is small compared to the total number of neutrino sources. The corresponding explanation for a non-detection of a UHECR-neutrino correlation is that the neutrino flux of sources in the local universe is too small to be detected with IceCube and ANTARES with the analyses presented here. The implications of a non-detection of a UHECR-neutrino correlation, based on earlier results in The IceCube Collaboration et al. (2016) and Schumacher (2019), has been studied in more detail in Palladino et al. (2020). In addition, the sources could be transient, such that the UHECRs emitted over a short period of time arrive much later due to their deflection, whereas the neutrinos travel on a straight path. It has been estimated by Davoudifar (2011) that the deflection in the EGMF causes a time delay on the order of a thousand years. Already a delay of a couple of decades is sufficient to de-correlate the observed UHECRs and neutrinos, as the livetime of the neutrino and UHECR data sets ranges between 7 and 13 years.

Another source of uncertainty is the mass composition and thus the charge of UHECRs at the highest energies. The measurements of the UHECR composition above ~ 50 EeV are not yet conclusive. However, several composition constraints at the highest energies (Aab et al. 2014a,b) and the lack of significant, magnetically-induced structures in the UHECR arrival directions (Aab et al. 2020) suggest that less than 10% of UHECRs above ~ 50 EeV might be light elements. Only the light UHECRs are expected to have their source in the vicinity of their arrival direction as derived from the benchmark deflection model. The sources of heavier UHECRs, e.g. iron nuclei, are spatially almost uncorrelated to the UHECR arrival directions due to the 26-times larger magnetic deflection compared to protons. We see in analysis 1 that the limits on the neutrino flux are significantly relaxed when assuming a correlation fraction of 50% or 10%. This correlation fraction, defined as the number of UHECRs with a neutrino source in their vicinity, is a simplified model of the UHECR composition.

The modeling of the magnetic deflection as a 2D Gaussian as assumed for analysis 1 and 2 is a simplification with respect to the PT11 and JF12 GMF models (Pshirkov et al. 2011; Jansson & Farrar 2012), which themselves are subject to large uncertainties. Especially in the region of the Galactic Plane, we expect deflections that are larger than the assumed mean value of around 3° . In addition, coherent deflection of UHECRs in the GMF or the deflection of UHECRs in the IGMF are not explicitly accounted for. Overall, a coherent shift of UHECRs depending on their arrival direction or an overall significantly larger deflection in the GMF and IGMF can dilute the spatial correlation of UHECRs and neutrinos. Nevertheless, a scaling of the overall deflection is covered partially with the scaling factor applied in analyses 1 and 2, since the overall strength of the deflection and the UHECR charge are largely degenerate parameters.

From a theoretical perspective, the connection of UHECRs and high-energy neutrinos is plausible based on their similar energy budget (Waxman & Bahcall 1999; Bahcall & Waxman 2001; Murase et al. 2013; Ahlers & Halzen 2018). However, neutrinos with energies in the TeV–PeV range originate most likely from cosmic rays with energies below ~ 100 PeV (Murase & Waxman 2016), which is below the energy threshold of > 50 EeV of the UHECR data sets used here. Furthermore, it is possible that efficient UHECR sources are less efficient neutrino sources and vice versa: Sources with efficient UHECR acceleration and emission require an optically thin proton and radiation environment, while sources with dense proton and radiation targets are efficient in neutrino production, but not in UHECR emission. Thus, different zones of UHECR acceleration and neutrino production are one possible model for common sources of UHECRs with $E > 50$ EeV and TeV–PeV neutrinos (Ahlers & Halzen 2018): Cosmic rays below ~ 100 PeV are confined in a calorimetric environment and subsequently produce TeV–PeV neutrinos, while a fraction of the cosmic rays are accelerated to the highest energies and escape the source before interacting (Murase & Waxman 2016; Ahlers & Halzen 2018). Such a model is yet to be proven, but the first indication of such a connection could be NGC 1068 as a potential neutrino source candidate (Aartsen et al. 2020b; Inoue et al. 2020) and UHECR source candidate (Aab et al. 2018). Dedicated future searches correlating UHECR, photon and neutrino observations are thus well motivated for proving such a connection.

The three analyses presented here reflect complementary approaches for tackling the question of a common origin of UHECRs and high-energy neutrinos. Despite substantially enlarged data sets and improved methods, the initially reported results in The IceCube Collaboration et al. (2016) could not be strengthened. For future analyses, we expect substantial gains in sensitivity if the charge of UHECR could be estimated on an event-by-event basis, as it is expected for future measurements by Auger Prime (Aab et al. 2016).

ACKNOWLEDGEMENTS

The authors of the ANTARES collaboration acknowledge the financial support of the funding agencies: Centre National de la Recherche Scientifique (CNRS), Commissariat à l'énergie atomique et aux énergies alternatives (CEA), Commission Européenne (FEDER fund and Marie Curie Program), Institut Universitaire de France (IUF), LabEx UnivEarthS (ANR-10-LABX-0023 and ANR-18-IDEX-0001), Région Île-de-France (DIM-ACAV), Région Alsace (contrat CPER), Région Provence-Alpes-Côte d'Azur, Département du Var and Ville de La Seyne-sur-Mer, France; Bundesministerium für Bildung und Forschung (BMBF), Germany; Istituto Nazionale di Fisica Nucleare (INFN), Italy; Nederlandse organisatie voor Wetenschappelijk Onderzoek (NWO), the Netherlands; Council of the President of the Russian Federation for young scientists and leading scientific schools supporting grants, Russia; Executive Unit for Financing Higher Education, Research, Development and Innovation (UEFISCDI), Romania; Ministerio de Ciencia, Innovación, Investigación y Universidades (MCIU): Programa Estatal de Generación de Conocimiento (refs. PGC2018-096663-B-C41, -A-C42, -B-C43, -B-C44) (MCIU/FEDER), Generalitat Valenciana: Prometeo (PROMETEO/2020/019), Grisolia (refs. GRISOLIA/2018/119, /2021/192) and GenT (refs. CIDEGENT/2018/034, /2019/043, /2020/049, /2021/023) programs, Junta de Andalucía (ref. A-FQM-053-UGR18), La Caixa Foundation (ref. LCF/BQ/IN17/11620019), EU: MSC program (ref. 101025085), Spain; Ministry of Higher Education, Scientific Research and Innovation, Morocco, and the Arab Fund for Economic and Social Development, Kuwait. We also acknowledge the technical support of Ifremer, AIM and Foselev Marine for the sea operation and the CC-IN2P3 for the computing facilities. The ANTARES collaboration acknowledges the significant contributions to this manuscript from Julien Aublin.

The IceCube collaboration acknowledges the significant contributions to this manuscript from Cyril Alispach, Anastasia Barbano and Lisa Schumacher. The authors of the IceCube Collaboration acknowledge the support from the following agencies: USA – U.S. National Science Foundation-Office of Polar Programs, U.S. National Science Foundation-Physics Division, U.S. National Science Foundation-EPSCoR, Wisconsin Alumni Research Foundation, Center for High Throughput Computing (CHTC) at the University of Wisconsin–Madison, Open Science Grid (OSG), Extreme Science and Engineering Discovery Environment (XSEDE), Frontera computing project at the Texas Advanced Computing Center, U.S. Department of Energy-National Energy Research Scientific Computing Center, Particle astrophysics research computing center at the University of Maryland, Institute for Cyber-Enabled Research at Michigan State University, and Astroparticle physics computational facility at Marquette University; Belgium – Funds for Scientific Research (FRS-FNRS and FWO), FWO Odysseus and Big Science programmes, and Belgian Federal Science Policy Office (Belspo); Germany – Bundesministerium für Bildung und Forschung (BMBF), Deutsche Forschungsgemeinschaft (DFG), Helmholtz Alliance for Astroparticle Physics (HAP), Initiative and Networking Fund of the Helmholtz Association, Deutsches Elektronen Synchrotron (DESY), and High Performance Computing cluster of the RWTH Aachen; Sweden – Swedish Research Council, Swedish Polar Research Secretariat, Swedish National Infrastructure for Computing (SNIC), and Knut and Alice Wallenberg Foundation; Australia – Australian Research Council; Canada – Natural Sciences and Engineering Research Council of Canada, Calcul Québec, Compute Ontario, Canada Foundation for Innovation, WestGrid, and Compute Canada; Denmark – Villum Fonden and Carlsberg Foundation;

New Zealand – Marsden Fund; Japan – Japan Society for Promotion of Science (JSPS) and Institute for Global Prominent Research (IGPR) of Chiba University; Korea – National Research Foundation of Korea (NRF); Switzerland – Swiss National Science Foundation (SNSF); United Kingdom – Department of Physics, University of Oxford. L.S. and C.H.W. acknowledge financial support from the "Deutsche Forschungsgemeinschaft".

The successful installation, commissioning, and operation of the Pierre Auger Observatory would not have been possible without the strong commitment and effort from the technical and administrative staff in Malargüe. We are very grateful to the following agencies and organizations for financial support:

Argentina – Comisión Nacional de Energía Atómica; Agencia Nacional de Promoción Científica y Tecnológica (ANPCyT); Consejo Nacional de Investigaciones Científicas y Técnicas (CONICET); Gobierno de la Provincia de Mendoza; Municipalidad de Malargüe; NDM Holdings and Valle Las Leñas; in gratitude for their continuing cooperation over land access; Australia – the Australian Research Council; Belgium – Fonds de la Recherche Scientifique (FNRS); Research Foundation Flanders (FWO); Brazil – Conselho Nacional de Desenvolvimento Científico e Tecnológico (CNPq); Financiadora de Estudos e Projetos (FINEP); Fundação de Amparo à Pesquisa do Estado de Rio de Janeiro (FAPERJ); São Paulo Research Foundation (FAPESP) Grants No. 2019/10151-2, No. 2010/07359-6 and No. 1999/05404-3; Ministério da Ciência, Tecnologia, Inovações e Comunicações (MCTIC); Czech Republic – Grant No. MSMT CR LTT18004, LM2015038, LM2018102, CZ.02.1.01/0.0/0.0/16_013/0001402, CZ.02.1.01/0.0/0.0/18_046/0016010 and CZ.02.1.01/0.0/0.0/17_049/0008422; France – Centre de Calcul IN2P3/CNRS; Centre National de la Recherche Scientifique (CNRS); Conseil Régional Ile-de-France; Département Physique Nucléaire et Corpusculaire (PNC-IN2P3/CNRS); Département Sciences de l’Univers (SDU-INSU/CNRS); Institut Lagrange de Paris (ILP) Grant No. LABEX ANR-10-LABX-63 within the Investissements d’Avenir Programme Grant No. ANR-11-IDEX-0004-02; Germany – Bundesministerium für Bildung und Forschung (BMBF); Deutsche Forschungsgemeinschaft (DFG); Finanzministerium Baden-Württemberg; Helmholtz Alliance for Astroparticle Physics (HAP); Helmholtz-Gemeinschaft Deutscher Forschungszentren (HGF); Ministerium für Innovation, Wissenschaft und Forschung des Landes Nordrhein-Westfalen; Ministerium für Wissenschaft, Forschung und Kunst des Landes Baden-Württemberg; Italy – Istituto Nazionale di Fisica Nucleare (INFN); Istituto Nazionale di Astrofisica (INAF); Ministero dell’Istruzione, dell’Università e della Ricerca (MIUR); CETEMPS Center of Excellence; Ministero degli Affari Esteri (MAE); México – Consejo Nacional de Ciencia y Tecnología (CONACYT) No. 167733; Universidad Nacional Autónoma de México (UNAM); PAPIIT DGAPA-UNAM; The Netherlands – Ministry of Education, Culture and Science; Netherlands Organisation for Scientific Research (NWO); Dutch national e-infrastructure with the support of SURF Cooperative; Poland – Ministry of Education and Science, grant No. DIR/WK/2018/11; National Science Centre, Grants No. 2016/22/M/ST9/00198, 2016/23/B/ST9/01635, and 2020/39/B/ST9/01398; Portugal – Portuguese national funds and FEDER funds within Programa Operacional Factores de Competitividade through Fundação para a Ciência e a Tecnologia (COMPETE); Romania – Ministry of Research, Innovation and Digitization, CNCS/CCCDI – UEFISCDI, projects PN19150201/16N/2019, PN1906010, TE128 and PED289, within PNCDI III; Slovenia – Slovenian Research Agency, grants P1-0031, P1-0385, I0-0033, N1-

0111; Spain – Ministerio de Economía, Industria y Competitividad (FPA2017-85114-P and PID2019-104676GB-C32), Xunta de Galicia (ED431C 2017/07), Junta de Andalucía (SOMM17/6104/UGR, P18-FR-4314) Feder Funds, RENATA Red Nacional Temática de Astropartículas (FPA2015-68783-REDT) and María de Maeztu Unit of Excellence (MDM-2016-0692); USA – Department of Energy, Contracts No. DE-AC02-07CH11359, No. DE-FR02-04ER41300, No. DE-FG02-99ER41107 and No. DE-SC0011689; National Science Foundation, Grant No. 0450696; The Grainger Foundation; Marie Curie-IRSES/EPLANET; European Particle Physics Latin American Network; and UNESCO.

The Telescope Array experiment is supported by the Japan Society for the Promotion of Science(JSPS) through Grants-in-Aid for Priority Area 431, for Specially Promoted Research JP21000002, for Scientific Research (S) JP19104006, for Specially Promoted Research JP15H05693, for Scientific Research (S) JP15H05741, for Science Research (A) JP18H03705, for Young Scientists (A) JPH26707011, and for Fostering Joint International Research (B) JP19KK0074, by the joint research program of the Institute for Cosmic Ray Research (ICRR), The University of Tokyo; by the Pioneering Program of RIKEN for the Evolution of Matter in the Universe (r-EMU); by the U.S. National Science Foundation awards PHY-1404495, PHY-1404502, PHY-1607727, PHY-1712517, PHY-1806797, PHY-2012934, and PHY-2112904; by the National Research Foundation of Korea (2017K1A4A3015188, 2020R1A2C1008230, & 2020R1A2C2102800) ; by the Ministry of Science and Higher Education of the Russian Federation under the contract 075-15-2020-778, IISN project No. 4.4501.18, and Belgian Science Policy under IUAP VII/37 (ULB). This work was partially supported by the grants of The joint research program of the Institute for Space-Earth Environmental Research, Nagoya University and Inter-University Research Program of the Institute for Cosmic Ray Research of University of Tokyo. The foundations of Dr. Ezekiel R. and Edna Wattis Dumke, Willard L. Eccles, and George S. and Dolores Doré Eccles all helped with generous donations. The State of Utah supported the project through its Economic Development Board, and the University of Utah through the Office of the Vice President for Research. The experimental site became available through the cooperation of the Utah School and Institutional Trust Lands Administration (SITLA), U.S. Bureau of Land Management (BLM), and the U.S. Air Force. We appreciate the assistance of the State of Utah and Fillmore offices of the BLM in crafting the Plan of Development for the site. Patrick A. Shea assisted the collaboration with valuable advice and supported the collaboration's efforts. The people and the officials of Millard County, Utah have been a source of steadfast and warm support for our work which we greatly appreciate. We are indebted to the Millard County Road Department for their efforts to maintain and clear the roads which get us to our sites. We gratefully acknowledge the contribution from the technical staffs of our home institutions. An allocation of computer time from the Center for High Performance Computing at the University of Utah is gratefully acknowledged.

Facility: ANTARES, IceCube Neutrino Observatory, Pierre Auger Observatory, Telescope Array

REFERENCES

- Aab, A., Abreu, P., Aglietta, M., et al. 2014a, Phys. Rev. D, 90, 122005, doi: [10.1103/PhysRevD.90.122005](https://doi.org/10.1103/PhysRevD.90.122005)
- . 2014b, Phys. Rev. D, 90, 122006, doi: [10.1103/PhysRevD.90.122006](https://doi.org/10.1103/PhysRevD.90.122006)

- Aab, A., Abreu, P., Aglietta, M., et al. 2015, *ApJ*, 804, 15, doi: [10.1088/0004-637X/804/1/15](https://doi.org/10.1088/0004-637X/804/1/15)
- . 2016, arXiv e-prints, arXiv:1604.03637, <https://arxiv.org/abs/1604.03637>
- . 2017, *Science*, 357, 1266, doi: [10.1126/science.aan4338](https://doi.org/10.1126/science.aan4338)
- Aab, A., Abreu, P., Aglietta, M., et al. 2018, *The Astrophysical Journal*, 853, L29, doi: [10.3847/2041-8213/aaa66d](https://doi.org/10.3847/2041-8213/aaa66d)
- Aab, A., Abreu, P., Aglietta, M., et al. 2020, *Journal of Instrumentation*, 15, P10021, doi: [10.1088/1748-0221/15/10/P10021](https://doi.org/10.1088/1748-0221/15/10/P10021)
- Aab, A., Abreu, P., Aglietta, M., et al. 2020, *Journal of Cosmology and Astroparticle Physics*, 2020, 017, doi: [10.1088/1475-7516/2020/06/017](https://doi.org/10.1088/1475-7516/2020/06/017)
- Aartsen, M. G., Abbasi, R., Ackermann, M., et al. 2014a, *Journal of Instrumentation*, 9, P03009, doi: [10.1088/1748-0221/9/03/P03009](https://doi.org/10.1088/1748-0221/9/03/P03009)
- Aartsen, M. G., Ackermann, M., Adams, J., et al. 2014b, *PhRvL*, 113, 101101, doi: [10.1103/PhysRevLett.113.101101](https://doi.org/10.1103/PhysRevLett.113.101101)
- . 2014c, *ApJ*, 796, 109, doi: [10.1088/0004-637X/796/2/109](https://doi.org/10.1088/0004-637X/796/2/109)
- Aartsen, M. G., Abraham, K., Ackermann, M., et al. 2016, *ApJ*, 833, 3, doi: [10.3847/0004-637X/833/1/3](https://doi.org/10.3847/0004-637X/833/1/3)
- . 2017a, *ApJ*, 835, 45, doi: [10.3847/1538-4357/835/1/45](https://doi.org/10.3847/1538-4357/835/1/45)
- Aartsen, M. G., Ackermann, M., Adams, J., et al. 2017b, *Journal of Instrumentation*, 12, P03012, doi: [10.1088/1748-0221/12/03/P03012](https://doi.org/10.1088/1748-0221/12/03/P03012)
- . 2017c, *Astroparticle Physics*, 92, 30, doi: [10.1016/j.astropartphys.2017.05.002](https://doi.org/10.1016/j.astropartphys.2017.05.002)
- Aartsen, M. G., Abraham, K., Ackermann, M., et al. 2017d, *ApJ*, 835, 151, doi: [10.3847/1538-4357/835/2/151](https://doi.org/10.3847/1538-4357/835/2/151)
- Aartsen, M. G., Ackermann, M., Adams, J., et al. 2018a, *Science*, 361, eaat1378, doi: [10.1126/science.aat1378](https://doi.org/10.1126/science.aat1378)
- . 2018b, *Science*, 361, 147, doi: [10.1126/science.aat2890](https://doi.org/10.1126/science.aat2890)
- . 2018c, *PhRvD*, 98, 062003, doi: [10.1103/PhysRevD.98.062003](https://doi.org/10.1103/PhysRevD.98.062003)
- . 2019, *European Physical Journal C*, 79, 234, doi: [10.1140/epjc/s10052-019-6680-0](https://doi.org/10.1140/epjc/s10052-019-6680-0)
- . 2020a, *PhRvL*, 125, 121104, doi: [10.1103/PhysRevLett.125.121104](https://doi.org/10.1103/PhysRevLett.125.121104)
- . 2020b, *PhRvL*, 124, 051103, doi: [10.1103/PhysRevLett.124.051103](https://doi.org/10.1103/PhysRevLett.124.051103)
- . 2020c, *ApJ*, 892, 53, doi: [10.3847/1538-4357/ab791d](https://doi.org/10.3847/1538-4357/ab791d)
- . 2020d, *ApJL*, 898, L10, doi: [10.3847/2041-8213/ab9d24](https://doi.org/10.3847/2041-8213/ab9d24)
- Abbasi, R., Abdou, Y., Ackermann, M., et al. 2013, *Nuclear Instruments and Methods in Physics Research A*, 700, 188, doi: [10.1016/j.nima.2012.10.067](https://doi.org/10.1016/j.nima.2012.10.067)
- Abbasi, R., Ackermann, M., Adams, J., et al. 2021, *PhRvD*, 104, 022002, doi: [10.1103/PhysRevD.104.022002](https://doi.org/10.1103/PhysRevD.104.022002)
- Abbasi, R. U., Abe, M., Abu-Zayyad, T., et al. 2014, *ApJL*, 790, L21, doi: [10.1088/2041-8205/790/2/L21](https://doi.org/10.1088/2041-8205/790/2/L21)
- . 2018, *ApJL*, 867, L27, doi: [10.3847/2041-8213/aaebf9](https://doi.org/10.3847/2041-8213/aaebf9)
- Abreu, P., Aglietta, M., Ahn, E. J., et al. 2011, arXiv e-prints, arXiv:1107.4809, <https://arxiv.org/abs/1107.4809>
- Abreu, P., Aglietta, M., Albury, J. M., et al. 2021, in *Proceedings of 37th International Cosmic Ray Conference — PoS(ICRC2021)*, Vol. 395, 307, doi: [10.22323/1.395.0307](https://doi.org/10.22323/1.395.0307)
- Abu-Zayyad, T., Aida, R., Allen, M., et al. 2012, *Nuclear Instruments and Methods in Physics Research A*, 689, 87, doi: [10.1016/j.nima.2012.05.079](https://doi.org/10.1016/j.nima.2012.05.079)
- Ageron, M., Aguilar, J. A., Al Samarai, I., et al. 2011, *Nuclear Instruments and Methods in Physics Research A*, 656, 11, doi: [10.1016/j.nima.2011.06.103](https://doi.org/10.1016/j.nima.2011.06.103)
- Aguilar, J. A., Albert, A., Ameli, F., et al. 2007, *Nuclear Instruments and Methods in Physics Research A*, 570, 107, doi: [10.1016/j.nima.2006.09.098](https://doi.org/10.1016/j.nima.2006.09.098)
- Ahlers, M., & Halzen, F. 2018, *Progress in Particle and Nuclear Physics*, 102, 73, doi: [10.1016/j.pnpnp.2018.05.001](https://doi.org/10.1016/j.pnpnp.2018.05.001)
- Albert, A., André, M., Anghinolfi, M., et al. 2017, *PhRvD*, 96, 082001, doi: [10.1103/PhysRevD.96.082001](https://doi.org/10.1103/PhysRevD.96.082001)
- . 2018, *ApJL*, 863, L30, doi: [10.3847/2041-8213/aad8c0](https://doi.org/10.3847/2041-8213/aad8c0)
- Albert, A., André, M., Anghinolfi, M., et al. 2020, *The Astrophysical Journal*, 892, 92, doi: [10.3847/1538-4357/ab7afb](https://doi.org/10.3847/1538-4357/ab7afb)
- Alves Batista, R., Biteau, J., Bustamante, M., et al. 2019, *Frontiers in Astronomy and Space Sciences*, 6, 23, doi: [10.3389/fspas.2019.00023](https://doi.org/10.3389/fspas.2019.00023)

- Anchordoqui, L. A., Hooper, D., Sarkar, S., & Taylor, A. M. 2008, *Astroparticle Physics*, 29, 1, doi: [10.1016/j.astropartphys.2007.10.006](https://doi.org/10.1016/j.astropartphys.2007.10.006)
- ANTARES Collaboration, Amram, P., Anghinolfi, M., et al. 2002, *Nuclear Instruments and Methods in Physics Research A*, 484, 369, doi: [10.1016/S0168-9002\(01\)02026-5](https://doi.org/10.1016/S0168-9002(01)02026-5)
- Aublin, J., Coleiro, A., Kouchner, A., et al. 2019, *EPJ Web Conf.*, 210, 03003, doi: [10.1051/epjconf/201921003003](https://doi.org/10.1051/epjconf/201921003003)
- Bahcall, J., & Waxman, E. 2001, *PhRvD*, 64, 023002, doi: [10.1103/PhysRevD.64.023002](https://doi.org/10.1103/PhysRevD.64.023002)
- Barbano, A. M. 2019, in *Proceedings of 36th International Cosmic Ray Conference — PoS(ICRC2019)*, Vol. 358, 842, doi: [10.22323/1.358.0842](https://doi.org/10.22323/1.358.0842)
- Biteau, J., Bister, T., Caccianiga, L., et al. 2019, in *European Physical Journal Web of Conferences*, Vol. 210, European Physical Journal Web of Conferences, 01005, doi: [10.1051/epjconf/201921001005](https://doi.org/10.1051/epjconf/201921001005)
- Bonifazi, C., & The Pierre Auger Collaboration. 2009, *Nuclear Physics B Proceedings Supplements*, 190, 20, doi: [10.1016/j.nuclphysbps.2009.03.063](https://doi.org/10.1016/j.nuclphysbps.2009.03.063)
- Davoudifar, P. 2011, in *32nd International Cosmic Ray Conference*, Vol. 2, 230, doi: [10.7529/ICRC2011/V02/1183](https://doi.org/10.7529/ICRC2011/V02/1183)
- Dawson, B. 2019, in *Proceedings of 36th International Cosmic Ray Conference — PoS(ICRC2019)*, Vol. 358, 231, doi: [10.22323/1.358.0231](https://doi.org/10.22323/1.358.0231)
- Durrer, R., & Neronov, A. 2013, *Astron. Astrophys. Rev.*, 21, 62, doi: [10.1007/s00159-013-0062-7](https://doi.org/10.1007/s00159-013-0062-7)
- Górski, K. M., Hivon, E., Banday, A. J., et al. 2005, *ApJ*, 622, 759, doi: [10.1086/427976](https://doi.org/10.1086/427976)
- Haack, C., & Wiebusch, C. 2017, in *Proceedings of 35th International Cosmic Ray Conference — PoS(ICRC2017)*, Vol. 301, 1005, doi: [10.22323/1.301.1005](https://doi.org/10.22323/1.301.1005)
- Illuminati, G., Aublin, J., & Navas, S. 2019, in *Proceedings of 36th International Cosmic Ray Conference — PoS(ICRC2019)*, Vol. 358, 920, doi: [10.22323/1.358.0920](https://doi.org/10.22323/1.358.0920)
- Inoue, Y., Khangulyan, D., & Doi, A. 2020, *The Astrophysical Journal*, 891, L33, doi: [10.3847/2041-8213/ab7661](https://doi.org/10.3847/2041-8213/ab7661)
- Jansson, R., & Farrar, G. R. 2012, *The Astrophysical Journal*, 757, 14, doi: [10.1088/0004-637X/757/1/14](https://doi.org/10.1088/0004-637X/757/1/14)
- Kawai, H., et al. 2008, *Nuclear Physics B - Proceedings Supplements*, 175-176, 221, doi: [10.1016/j.nuclphysbps.2007.11.002](https://doi.org/10.1016/j.nuclphysbps.2007.11.002)
- Kopper, C. 2017, in *Proceedings of 35th International Cosmic Ray Conference — PoS(ICRC2017)*, Vol. 301, 981, doi: [10.22323/1.301.0981](https://doi.org/10.22323/1.301.0981)
- Kronberg, P. P. 1994, *Rept. Prog. Phys.*, 57, 325, doi: [10.1088/0034-4885/57/4/001](https://doi.org/10.1088/0034-4885/57/4/001)
- Meszaros, P. 2018, *PhT*, 71, 36
- Murase, K. 2015, *AIP Conference Proceedings*, 1666, 040006, doi: [10.1063/1.4915555](https://doi.org/10.1063/1.4915555)
- Murase, K., Ahlers, M., & Lacki, B. C. 2013, *Physical Review D*, 88, 121301, doi: [10.1103/PhysRevD.88.121301](https://doi.org/10.1103/PhysRevD.88.121301)
- Murase, K., & Waxman, E. 2016, *Physical Review D*, 94, 103006, doi: [10.1103/PhysRevD.94.103006](https://doi.org/10.1103/PhysRevD.94.103006)
- Nagano, M., & Watson, A. A. 2000, *Reviews of Modern Physics*, 72, 689, doi: [10.1103/RevModPhys.72.689](https://doi.org/10.1103/RevModPhys.72.689)
- Paiano, S., Falomo, R., Treves, A., & Scarpa, R. 2018, *ApJL*, 854, L32, doi: [10.3847/2041-8213/aaad5e](https://doi.org/10.3847/2041-8213/aaad5e)
- Palladino, A., van Vliet, A., Winter, W., & Franckowiak, A. 2020, *Monthly Notices of the Royal Astronomical Society*, 494, 4255, doi: [10.1093/mnras/staa1003](https://doi.org/10.1093/mnras/staa1003)
- Particle Data Group, Zyla, P. A., Barnett, R. M., et al. 2020, *Progress of Theoretical and Experimental Physics*, 2020, 083C01, doi: [10.1093/ptep/ptaa104](https://doi.org/10.1093/ptep/ptaa104)
- Pshirkov, M. S., Tinyakov, P. G., Kronberg, P. P., & Newton-McGee, K. J. 2011, *The Astrophysical Journal*, 738, 192, doi: [10.1088/0004-637X/738/2/192](https://doi.org/10.1088/0004-637X/738/2/192)
- Pshirkov, M. S., Tinyakov, P. G., & Urban, F. R. 2016, *Phys. Rev. Lett.*, 116, 191302, doi: [10.1103/PhysRevLett.116.191302](https://doi.org/10.1103/PhysRevLett.116.191302)
- Schumacher, L. 2019, in *European Physical Journal Web of Conferences*, Vol. 207, European Physical Journal Web of Conferences, 02010, doi: [10.1051/epjconf/201920702010](https://doi.org/10.1051/epjconf/201920702010)
- Sommers, P. 2001, *Astroparticle Physics*, 14, 271, doi: [10.1016/S0927-6505\(00\)00130-4](https://doi.org/10.1016/S0927-6505(00)00130-4)

- Stettner, J. 2019, in Proceedings of 36th International Cosmic Ray Conference — PoS(ICRC2019), Vol. 358, 1017, doi: [10.22323/1.358.1017](https://doi.org/10.22323/1.358.1017)
- The IceCube Collaboration. 2013, *Science*, 342, 1242856, doi: [10.1126/science.1242856](https://doi.org/10.1126/science.1242856)
- The IceCube Collaboration, The Pierre Auger Collaboration, & The Telescope Array Collaboration. 2016, *JCAP*, 2016, 037, doi: [10.1088/1475-7516/2016/01/037](https://doi.org/10.1088/1475-7516/2016/01/037)
- The Pierre Auger Collaboration. 2015, *Nuclear Instruments and Methods in Physics Research A*, 798, 172, doi: [10.1016/j.nima.2015.06.058](https://doi.org/10.1016/j.nima.2015.06.058)
- Tkachev, I., Fujii, T., Ivanov, D., et al. 2021, in Proceedings of 37th International Cosmic Ray Conference — PoS(ICRC2021), Vol. 395, 392, doi: [10.22323/1.395.0392](https://doi.org/10.22323/1.395.0392)
- Tokuno, H., Tameda, Y., Takeda, M., et al. 2012, *Nuclear Instruments and Methods in Physics Research A*, 676, 54, doi: [10.1016/j.nima.2012.02.044](https://doi.org/10.1016/j.nima.2012.02.044)
- Troitsky, S., Fukushima, M., Ikeda, D., et al. 2017, in Proceedings of 35th International Cosmic Ray Conference — PoS(ICRC2017), Vol. 301, 548, doi: [10.22323/1.301.0548](https://doi.org/10.22323/1.301.0548)
- Wandkowsky, N. 2018, in XXVIII International Conference on Neutrino Physics and Astrophysics, 501, doi: [10.5281/zenodo.1301088](https://doi.org/10.5281/zenodo.1301088)
- Waxman, E., & Bahcall, J. N. 1999, *Physical Review D*, 59, 023002, doi: [10.1103/PhysRevD.59.023002](https://doi.org/10.1103/PhysRevD.59.023002)